

Vibrational cavity modes in a free cylindrical disk

Shin-ichiro Tamura

Department of Applied Physics, Hokkaido University, Sapporo 060-8628, Japan

(Received 18 November 2008; published 12 February 2009)

We analyze theoretically the vibrational properties of a free cylindrical elastic disk of thickness $2h$ and radius a . In particular, the acoustic cavity modes, i.e., the low-lying resonant vibrations with a large angular wave number n ($=2\pi a/\lambda \sim 20$, with λ as the wavelength) along the circumference are considered. These modes are either confined at the corners between the sidewall and the top and bottom planes of the disk (the edge modes), or trapped near the circumference of the cylinder (the surface modes). They are understood as the modes modified from the whispering-gallery and Rayleigh waves on the curved surface of an infinitely long cylinder by the presence of the stress-free end planes. Small mode volumes occupied by these vibrations and their expected large quality factors in the disk with smooth boundary surfaces make the cavity modes attractive for the fundamental studies as well as for the applications to micro- and nanophononics. The mathematical formulation follows the works originally developed by Rasband [J. Acoust. Soc. Am. **57**, 899 (1975)] and Hutchinson [J. Appl. Mech. **47**, 901 (1980)]. Numerical examples are presented for polycrystalline aluminum disks with aspect ratios $h/a=0.5$ and 0.05 .

DOI: [10.1103/PhysRevB.79.054302](https://doi.org/10.1103/PhysRevB.79.054302)

PACS number(s): 62.65.+k, 62.25.-g, 62.30.+d, 68.35.Ja

I. INTRODUCTION

The vibrational properties of small elastic structures down to nanometer scales have recently attracted much attention.¹⁻⁴ In particular, three-dimensional (3D) confinement of high-frequency acoustic vibrations from 1 GHz to 1 THz range inside small structures is important in the development of micro- and nanophononics and related fields. Possible applications are the manipulation and control of light and electrons in acousto-optical and electromechanical devices.⁵⁻⁸ A more interesting potential application should be a design of resonant acoustic cavities for the sound laser, or sound amplification of stimulated emission of radiation (SASER), i.e., the acoustic analog of a laser, of small scales.⁹ Similar idea for the confinement of light inside microstructures has already been applied to the realization of optical cavities for miniaturized semiconductor lasers.¹⁰ Several structures such as microspheres, microdisks, and micropillars which support the optical cavity modes [whispering-gallery (WG) modes] with very large quality (Q) factor have been fabricated.¹¹⁻¹⁴ However, the vibrational properties of the confined vibrational cavity modes in the same structures have not fully been investigated. Here we note that a prototype of the SASER device has a pillar structure of a nanometer dimension consisting of alternate stacks of semiconducting heterolayers.

Similar to the cases of the optical cavity modes, we may also expect large Q factors for the vibrational resonant modes in micro- and nanoacoustic cavities if the surfaces or interfaces are controlled to be so smooth that the lifetimes of the resonances against scattering by roughness may be suppressed to be small. The small spatial volume occupied by these highly confined modes inside the cavity and the expected low acoustical dissipation rate make these vibrational modes attractive for the fundamental studies and also for a wide range of applications to new phononic and electromechanical devices.

Here we note that in those micro- and nanostructures, the acoustical vibrations trapped in a small volume should be

deeply related to the Rayleigh-type surface (RS) waves that propagate in the vicinity of the boundary surfaces.^{15,16} In addition, there exists another mode of waves that propagate by repeating total internal reflections at the curved boundaries, i.e., the WG waves.^{17,18} It should be noted that the WG waves were originally found as the mode of longitudinal sound circulating in the air filled inside a cylindrical (or a spherical) space along the rigid circumferential wall. The optical cavity modes widely studied recently are the electromagnetic equivalent of the WG waves. Thus, in a small circular 3D structure, the vibrational cavity modes should be essentially the RS and WG waves but they may be modulated drastically by the geometry of the cavity designed.

Before studying the elastic cavities with rather complicated heterostructures, such as pillars with multilayered structures, we consider in the present work the simplest 3D cavity structure for sound resonators, i.e., a free circular disk of thickness $2h$ and radius a (with the aspect ratio $h/a \leq 1$) with stress-free surfaces. Specifically, we will search for the low-lying resonant acoustic vibrations whose strain energies are stored in small volumes in the vicinity of the top, bottom, and circumferential surfaces of the disk.^{19,20} This happens for the modes with a large angular wave number n (>10) along the circumference because the centrifugal force for the waves with large n push them toward the boundary surface. This can be also seen by the fact that the angular wave number n characterizes the order of the Bessel function $J_n(x)$ (of the first kind) which governs the radial dependence of the vibrational amplitudes, and the smallest nonzero x giving its extremum, or satisfying $J'_n(x)=0$, is given by $x=n+o(n^{1/3})$.

The problem of obtaining eigenfrequencies of a vibrating circular cylinder with stress-free surfaces has so far been studied repeatedly and both the approximate and analytic solutions have been presented by many authors. A brief summary has been given in literature.²¹ Also several numerical schemes such as the basis function methods²² and the finite element methods²³ have been applied for obtaining frequency spectra of a variety of elastic objects with free

boundaries. In the present work we will employ the mathematical approach developed by Rasband²¹ and also by Hutchinson^{24,25} in a simpler way for solving analytically the vibrations in a free cylinder of a finite thickness.

The method of Hutchinson^{24,25} consists of combining three (essentially two) series of exact solutions for the equations of motion of the lattice displacement, which term by term satisfy *three* of six stress-free boundary conditions (three at the top and bottom planes and three at the side surface).^{25,26} The remaining *three* boundary conditions are satisfied by requiring that the stresses are orthogonal to appropriate complete orthogonal sets of functions. (This is equivalent to expanding the relevant stresses in a Fourier series in the axial direction and in a Fourier-Bessel series in the radial direction.) This procedure leads to a set of linear homogeneous equations to be solved for the amplitude vector of the lattice displacement. The resonant frequencies of the disk are then obtained by searching for the zeros of the determinant of the coefficient matrix with its rank determined by the number of functions kept in each complete set.

The present study for a freestanding cylindrical disk should provide a basis for analyzing further the vibrations of more complicated elastic structures such as a circular disk embedded in a dissimilar elastic matrix and a pillar consisting of periodic stackings of two-component circular disks with or without a foreign (an impurity) layer.

In Sec. II, we give two kinds of expressions for the solutions of the wave equations for the lattice and stress tensors with cylindrical coordinates. In Sec. III, for pedagogical purposes, we explain rather in detail how the stress-free boundary conditions are satisfied at the surfaces of the cylindrical disk. The expressions of the matrix elements from which the resonant frequencies are calculated are given in Sec. IV. Numerical examples are developed in Sec. V and the results are summarized in Sec. VI.

II. EQUATIONS OF MOTION

The equations of motion for the lattice displacement \mathbf{u} in an isotropic, elastic continuum are given by

$$\rho \ddot{\mathbf{u}} = (\lambda + 2\mu) \nabla (\nabla \cdot \mathbf{u}) - \mu \nabla \times (\nabla \times \mathbf{u}), \quad (1)$$

where ρ is the mass density, and λ and μ are the Lamé coefficients. If we introduce a scalar potential ϕ_1 and two vector potentials $\boldsymbol{\psi}_J = \phi_J \mathbf{e}_z$ ($J=2,3$) through the scalar potentials ϕ_2 and ϕ_3 satisfying the wave equations

$$\ddot{\phi}_1 = v_l^2 \Delta \phi_1, \quad (2)$$

$$\ddot{\boldsymbol{\psi}}_J = v_t^2 \Delta \boldsymbol{\psi}_J \text{ or } \ddot{\phi}_J = v_t^2 \Delta \phi_J \quad (J=2,3), \quad (3)$$

with $v_l^2 = (\lambda + 2\mu)/\rho$ and $v_t^2 = \mu/\rho$ as the velocities of the longitudinal and transverse waves, the displacement vector \mathbf{u} satisfying Eq. (1) is expressed as

$$\begin{aligned} \mathbf{u} &= \nabla \phi_1 + \nabla \times \boldsymbol{\psi}_2 + \nabla \times \nabla \times \boldsymbol{\psi}_3 \\ &= \nabla \phi_1 + \nabla \times (\phi_2 \mathbf{e}_z) + \nabla \times \nabla \times (\phi_3 \mathbf{e}_z), \end{aligned} \quad (4)$$

with \mathbf{e}_z as the unit vector in the z direction. The first term is

the longitudinal (l) vibration and the second and third terms are the transverse (t) vibrations. So, we may use alternative symbols l and t for the indices $J=1=l$, $J=2=t$, and $J=3=t$ to show more explicitly the polarizations of these waves.

With the cylindrical coordinates, wave equations (2) and (3) are summarized as

$$\ddot{\phi}_J = v_J^2 \left[\frac{1}{r} \frac{\partial}{\partial r} \left(r \frac{\partial \phi_J}{\partial r} \right) + \frac{1}{r^2} \frac{\partial^2 \phi_J}{\partial \theta^2} + \frac{\partial^2 \phi_J}{\partial z^2} \right] \quad (5)$$

and the displacement components are explicitly written as

$$u_r = \frac{\partial \phi_1}{\partial r} + \frac{1}{r} \frac{\partial \phi_2}{\partial \theta} + \frac{\partial^2 \phi_3}{\partial r \partial z}, \quad (6)$$

$$u_\theta = \frac{1}{r} \frac{\partial \phi_1}{\partial \theta} - \frac{\partial \phi_2}{\partial r} + \frac{1}{r} \frac{\partial^2 \phi_3}{\partial \theta \partial z}, \quad (7)$$

$$u_z = \frac{\partial \phi_1}{\partial z} - \frac{\partial^2 \phi_3}{\partial r^2} - \frac{1}{r} \frac{\partial \phi_3}{\partial r} - \frac{1}{r^2} \frac{\partial^2 \phi_3}{\partial \theta^2}. \quad (8)$$

Here we note that the cylindrical disk studied has two kinds of boundary surfaces, i.e., the circumferential and flat (top and bottom) surfaces perpendicular to the r and z directions, respectively. If the disk is homogeneous and extended infinitely along the radial (r) direction, the wave number k in this direction is a conserved quantity and common to all three modes of vibrations but the wave number along the axial (z) direction depends on the mode. In contrast, if the system is extended infinitely along the axial direction, the wave number q in this direction is common to all modes but the wave number along the radial direction depends on each mode. However, the cylindrical disk is finite in both the radial and axial directions and hence the wave numbers k and q are not conserved quantities (the waves with $+k$ and $-k$ are mixed and so on) but can still be used to classify the vibrations. Thus, we adopt two sets of exact solutions of the wave equations obtained by assuming the wave numbers k and q are common to all three modes. They are explicitly given in Secs. II A and II B.

A. Solutions of the wave equations and stress tensor components: Case I

Now we choose the solutions of wave equations (2) and (3) of the forms (we refer to the upper and lower solutions in parentheses as the *even* and *odd* solutions, respectively)²⁷

$$\phi_{J=1} = R_1(k,r) \begin{pmatrix} \cos qz \\ \sin qz \end{pmatrix} \cos n\theta e^{-i\omega t}, \quad (9)$$

$$\phi_{J=2} = -R_2(k,r) \begin{pmatrix} \cos qz \\ \sin qz \end{pmatrix} \sin n\theta e^{-i\omega t}, \quad (10)$$

$$\phi_{J=3} = R_3(k,r) \begin{pmatrix} -\sin qz \\ \cos qz \end{pmatrix} \cos n\theta e^{-i\omega t}, \quad (11)$$

where ω is an angular frequency, n is an integer, and k_J and q are the wave numbers in the radial and axial directions

satisfying the dispersion relations $(\omega/v_j)^2 = k_j^2 + q^2$ (*case I*). It should be noted that the wave number q is common to the three potentials ϕ_j for *case I*. The equations satisfied by the radial part R_j are as follows:

(1) If the wave number k_j is real, or $k_j^2 = (\omega/v_j)^2 - q^2 > 0$, we have

$$R_j'' + \frac{1}{k_j r} R_j' + \left[1 - \left(\frac{n}{k_j r} \right)^2 \right] R_j = 0 \quad (12)$$

and the solution finite at $r=0$ is $R_j = J_n(k_j r)$, i.e., the Bessel function of the first kind.

(2) If the wave number k_j is pure imaginary, or $k_j^2 = (\omega/v_j)^2 - q^2 = -\kappa_j^2 < 0$, we set $\kappa_j = ik_j$ and obtain

$$R_j'' + \frac{1}{\kappa_j r} R_j' - \left[1 + \left(\frac{n}{\kappa_j r} \right)^2 \right] R_j = 0. \quad (13)$$

The solution finite at $r=0$ is the modified Bessel function $R_j = I_n(\kappa_j r) = i^{-n} J_n(ik_j r)$. It should be remarked that $J_0(0) = I_0(0) = 1$ and $J_n(0) = I_n(0) = 0$ for $n \geq 1$.

Thus, for real k_j we have $R_1 = J_n(k_1 r)$ and $R_2 = R_3 = J_n(k_r r)$ apart from constant coefficients, and the displacement vector $\mathbf{u} = (u_r, u_\theta, u_z)^t$ takes the form

$$\begin{pmatrix} u_r \\ u_\theta \\ u_z \end{pmatrix} = X_n(r, \theta, z) e^{-i\omega t} \begin{pmatrix} A_1 \\ A_2 \\ A_3 \end{pmatrix} \equiv X_n(r, \theta, z) e^{-i\omega t} \mathbf{A}, \quad (14)$$

where $\mathbf{A} = (A_1, A_2, A_3)^t$ is a constant vector (an amplitude vector) and

$$X_n(r, \theta, z) = \begin{pmatrix} k_r J_n'(k_r r) \begin{pmatrix} \cos qz \\ \sin qz \end{pmatrix} \cos n\theta & -\frac{n}{r} J_n(k_r r) \begin{pmatrix} \cos qz \\ \sin qz \end{pmatrix} \cos n\theta & -q k_r J_n'(k_r r) \begin{pmatrix} \cos qz \\ \sin qz \end{pmatrix} \cos n\theta \\ -\frac{n}{r} J_n(k_r r) \begin{pmatrix} \cos qz \\ \sin qz \end{pmatrix} \sin n\theta & k_r J_n'(k_r r) \begin{pmatrix} \cos qz \\ \sin qz \end{pmatrix} \sin n\theta & \frac{nq}{r} J_n(k_r r) \begin{pmatrix} \cos qz \\ \sin qz \end{pmatrix} \sin n\theta \\ q J_n(k_r r) \begin{pmatrix} -\sin qz \\ \cos qz \end{pmatrix} \cos n\theta & 0 & k_r^2 J_n(k_r r) \begin{pmatrix} -\sin qz \\ \cos qz \end{pmatrix} \cos n\theta \end{pmatrix}. \quad (15)$$

With this solution for the displacement vector \mathbf{u} , the stress components $(T_{rr}, T_{r\theta}, T_{rz})^t$ acting on the cylindrical surface and the stress components $(T_{zr}, T_{z\theta}, T_{zz})^t$ acting on the top and bottom faces of the cylindrical disk are given by

$$\begin{pmatrix} T_{rr} \\ T_{r\theta} \\ T_{rz} \end{pmatrix} = \begin{pmatrix} (\lambda + 2\mu) \frac{\partial}{\partial r} + \frac{\lambda}{r} & \frac{\lambda}{r} \frac{\partial}{\partial \theta} & \lambda \frac{\partial}{\partial z} \\ \frac{\mu}{r} \frac{\partial}{\partial \theta} & \mu \left(\frac{\partial}{\partial r} - \frac{1}{r} \right) & 0 \\ \mu \frac{\partial}{\partial z} & 0 & \mu \frac{\partial}{\partial r} \end{pmatrix} \begin{pmatrix} u_r \\ u_\theta \\ u_z \end{pmatrix} \\ \equiv 2\mu S_n^r(r, \theta, z) e^{-i\omega t} \mathbf{A}, \quad (16)$$

$$\begin{pmatrix} T_{zr} \\ T_{z\theta} \\ T_{zz} \end{pmatrix} = \begin{pmatrix} \mu \frac{\partial}{\partial z} & 0 & \mu \frac{\partial}{\partial r} \\ 0 & \mu \frac{\partial}{\partial z} & \frac{\mu}{r} \frac{\partial}{\partial \theta} \\ \lambda \left(\frac{\partial}{\partial r} + \frac{1}{r} \right) & \frac{\lambda}{r} \frac{\partial}{\partial \theta} & (\lambda + 2\mu) \frac{\partial}{\partial z} \end{pmatrix} \begin{pmatrix} u_r \\ u_\theta \\ u_z \end{pmatrix} \\ \equiv 2\mu S_n^z(r, \theta, z) e^{-i\omega t} \mathbf{A}, \quad (17)$$

where the expressions for the elements of the matrices S_n^r and S_n^z are lengthy and given in Appendix A.

B. Alternative forms for the solutions of the wave equations and stress tensor components: Case II

In Sec. II A we chose the axial wave number q common to three scalar potentials. Instead, we may choose the radial wave number k common to three scalar potentials. Setting $k_j = k_r = k$ and changing the wave number q to q_l and q_t , with $q_j^2 = (\omega/v_j)^2 - k^2$ (*case II*), we have alternative forms for the potentials

$$\phi_1 = J_n(kr) \begin{pmatrix} \cos q_l z \\ \sin q_l z \end{pmatrix} \cos n\theta e^{-i\omega t}, \quad (18)$$

$$\phi_2 = -J_n(kr) \begin{pmatrix} \cos q_t z \\ \sin q_t z \end{pmatrix} \sin n\theta e^{-i\omega t}, \quad (19)$$

$$\phi_3 = J_n(kr) \begin{pmatrix} -\sin q_t z \\ \cos q_t z \end{pmatrix} \cos n\theta e^{-i\omega t} \quad (20)$$

and the expression for the displacement vector \mathbf{u} is

$$\begin{pmatrix} u_r \\ u_\theta \\ u_z \end{pmatrix} = \tilde{X}_n(r, \theta, z) e^{-i\omega t} \begin{pmatrix} \tilde{B}_1 \\ \tilde{B}_2 \\ \tilde{B}_3 \end{pmatrix} \equiv \tilde{X}_n(r, \theta, z) e^{-i\omega t} \tilde{\mathbf{B}}, \quad (21)$$

where $\tilde{\mathbf{B}} = (\tilde{B}_1, \tilde{B}_2, \tilde{B}_3)^t$ is the amplitude vector and

$$\tilde{X}_n(r, \theta, z) = \begin{pmatrix} kJ'_n(kr) \begin{pmatrix} \cos q_1 z \\ \sin q_1 z \end{pmatrix} \cos n\theta & -\frac{n}{r} J_n(kr) \begin{pmatrix} \cos q_1 z \\ \sin q_1 z \end{pmatrix} \cos n\theta & -q_1 k J'_n(kr) \begin{pmatrix} \cos q_1 z \\ \sin q_1 z \end{pmatrix} \cos n\theta \\ -\frac{n}{r} J_n(kr) \begin{pmatrix} \cos q_1 z \\ \sin q_1 z \end{pmatrix} \sin n\theta & kJ'_n(kr) \begin{pmatrix} \cos q_1 z \\ \sin q_1 z \end{pmatrix} \sin n\theta & \frac{nq_1}{r} J_n(kr) \begin{pmatrix} \cos q_1 z \\ \sin q_1 z \end{pmatrix} \sin n\theta \\ q_1 J_n(kr) \begin{pmatrix} -\sin q_1 z \\ \cos q_1 z \end{pmatrix} \cos n\theta & 0 & k^2 J_n(kr) \begin{pmatrix} -\sin q_1 z \\ \cos q_1 z \end{pmatrix} \cos n\theta \end{pmatrix}. \quad (22)$$

With these expressions for the displacement vector, the relevant stresses are again written as

$$\begin{pmatrix} T_{rr} \\ T_{r\theta} \\ T_{rz} \end{pmatrix} = 2\mu \tilde{S}_n^r(r, \theta, z) e^{-i\omega t} \tilde{\mathbf{B}}, \quad (23)$$

$$\begin{pmatrix} T_{zr} \\ T_{z\theta} \\ T_{zz} \end{pmatrix} = 2\mu \tilde{S}_n^z(r, \theta, z) e^{-i\omega t} \tilde{\mathbf{B}} \quad (24)$$

and the matrix elements of \tilde{S}_n^r and \tilde{S}_n^z are given in Appendix B.

III. BOUNDARY CONDITIONS

For a free cylindrical disk with radius a and thickness $2h$, the stress-free boundary conditions are

$$T_{rr}(a, \theta, z) = 0, \quad (25)$$

$$T_{r\theta}(a, \theta, z) = 0, \quad (26)$$

$$T_{rz}(a, \theta, z) = 0 \quad (27)$$

on the circumference and

$$T_{zr}(r, \theta, \pm h) = 0, \quad (28)$$

$$T_{z\theta}(r, \theta, \pm h) = 0, \quad (29)$$

$$T_{zz}(r, \theta, \pm h) = 0 \quad (30)$$

on the top and bottom faces of the disk. However, as we will see below, it is not possible to satisfy identically all these boundary conditions by the eigensolutions of the wave equations given by Eqs. (14) and (21). So the following mathematical procedures employed are somewhat cumbersome.

First, we try to make a suitable superposition of displacement vectors (14) and (21). For instance, we set for u_r

$$u_r(r, \theta, z) = (X_n)_{11} A_1 + (X_n)_{12} A_2 + (X_n)_{13} A_3 + (\tilde{X}_n)_{11} \tilde{B}_1 + (\tilde{X}_n)_{12} \tilde{B}_2 + (\tilde{X}_n)_{13} \tilde{B}_3. \quad (31)$$

For the expression of u_θ and u_z , we may change $(X_n)_{1\beta}$ ($\beta=1, 2, 3$) to $(X_n)_{2\beta}$ and $(X_n)_{3\beta}$, respectively, and also similar changes should be done for $(\tilde{X}_n)_{1\beta}$. In this scheme, the stress tensor components are expressed as

$$T_{rr}(r, \theta, z)/2\mu = (S_n^r)_{11} A_1 + (S_n^r)_{12} A_2 + (S_n^r)_{13} A_3 + (\tilde{S}_n^r)_{11} \tilde{B}_1 + (\tilde{S}_n^r)_{12} \tilde{B}_2 + (\tilde{S}_n^r)_{13} \tilde{B}_3, \quad (32)$$

$$T_{zr}(r, \theta, z)/2\mu = (S_n^z)_{11} A_1 + (S_n^z)_{12} A_2 + (S_n^z)_{13} A_3 + (\tilde{S}_n^z)_{11} \tilde{B}_1 + (\tilde{S}_n^z)_{12} \tilde{B}_2 + (\tilde{S}_n^z)_{13} \tilde{B}_3, \quad (33)$$

and so on.

Here we note that the superpositions of the two types of exact solutions for the lattice displacements [Eq. (31) for u_r and so on] have six unknown amplitude coefficients which can be determined uniquely from six boundary conditions at the boundary surfaces, in principle. However, three of these boundary conditions are given at $r=a$ and the other three are at $z=\pm h$ and should be satisfied over the whole ranges $-h < z < h$ for the former three and over $0 < r < a$ for the latter three (θ dependence is factored out and does not cause any problem). Thus, the exact fulfillment of the boundary conditions at the curved and flat surfaces is not straightforward.

In order to overcome this difficulty, Rasband²¹ and Hutchinson²⁵ required partial fulfillment of *three* (for example, but not on the same surface) of six stress-free boundary conditions. The remaining *three* boundary conditions are then satisfied by requiring that the stresses are orthogonal to a relevant complete orthogonal set of functions in the radial (r) or the axial (z) direction. We follow these ideas and the associated mathematical procedures are described below.

A. First set of boundary conditions

First we require that the following three boundary conditions are satisfied *identically*:

$$T_{rz}(a, \theta, z) = 0, \quad (34)$$

$$T_{zr}(r, \theta, \pm h) = 0, \quad (35)$$

$$T_{z\theta}(r, \theta, \pm h) = 0. \quad (36)$$

Because $T_{rz}(a, \theta, z)$, $T_{zr}(r, \theta, h)$, and $T_{z\theta}(r, \theta, h)$ are explicitly written as

$$\begin{aligned} \frac{T_{rz}(a, \theta, z)}{2\mu \cos n\theta} = & \left[qk_l J'_n(k_l a) A_1 - \frac{nq}{2a} J_n(k_l a) A_2 + \frac{1}{2} k_l (k_l^2 - q^2) J'_n(k_l a) A_3 \right] \begin{pmatrix} -\sin qz \\ \cos qz \end{pmatrix} \\ & + \left[qk_l \begin{pmatrix} -\sin q_l z \\ \cos q_l z \end{pmatrix} \tilde{B}_1 + \frac{1}{2} k_l (k_l^2 - q_l^2) \begin{pmatrix} -\sin q_l z \\ \cos q_l z \end{pmatrix} \tilde{B}_3 \right] J'_n(ka) - \frac{nq_l}{2a} J_n(ka) \begin{pmatrix} -\sin q_l z \\ \cos q_l z \end{pmatrix} \tilde{B}_2, \end{aligned} \quad (37)$$

$$\begin{aligned} \frac{T_{rz}(r, \theta, h)}{2\mu \cos n\theta} = & \left[qk_l J'_n(k_l r) A_1 - \frac{nq}{2r} J_n(k_l r) A_2 + \frac{1}{2} k_l (k_l^2 - q^2) J'_n(k_l r) A_3 \right] \begin{pmatrix} -\sin qh \\ \cos qh \end{pmatrix} \\ & + \left[qk_l \begin{pmatrix} -\sin q_l h \\ \cos q_l h \end{pmatrix} \tilde{B}_1 + \frac{1}{2} k_l (k_l^2 - q_l^2) \begin{pmatrix} -\sin q_l h \\ \cos q_l h \end{pmatrix} \tilde{B}_3 \right] J'_n(kr) - \frac{nq_l}{2r} J_n(kr) \begin{pmatrix} -\sin q_l h \\ \cos q_l h \end{pmatrix} \tilde{B}_2, \end{aligned} \quad (38)$$

$$\begin{aligned} \frac{T_{z\theta}(r, \theta, h)}{2\mu \sin n\theta} = & - \left[\frac{nq}{r} J_n(k_l r) A_1 - \frac{qk_l}{2} J'_n(k_l r) A_2 + \frac{n}{2r} (k_l^2 - q^2) J_n(k_l r) A_3 \right] \begin{pmatrix} -\sin qh \\ \cos qh \end{pmatrix} \\ & - \left[\frac{nq_l}{r} \begin{pmatrix} -\sin q_l h \\ \cos q_l h \end{pmatrix} \tilde{B}_1 + \frac{n}{2r} (k_l^2 - q_l^2) \begin{pmatrix} -\sin q_l h \\ \cos q_l h \end{pmatrix} \tilde{B}_3 \right] J_n(kr) + \frac{q_l k}{2} J'_n(kr) \begin{pmatrix} -\sin q_l h \\ \cos q_l h \end{pmatrix} \tilde{B}_2, \end{aligned} \quad (39)$$

we impose the following conditions so that Eqs. (37)–(39) may vanish *term by term*:

$$qk_l J'_n(k_l a) A_1 - \frac{nq}{2a} J_n(k_l a) A_2 + \frac{1}{2} k_l (k_l^2 - q^2) J'_n(k_l a) A_3 = 0, \quad (40)$$

$$\tilde{B}_2 = 0, \quad (41)$$

$$J'_n(ka) = 0, \quad (42)$$

$$\begin{pmatrix} -\sin qh \\ \cos qh \end{pmatrix} = 0, \quad (43)$$

$$q_l \begin{pmatrix} -\sin q_l h \\ \cos q_l h \end{pmatrix} \tilde{B}_1 + \frac{1}{2} (k_l^2 - q_l^2) \begin{pmatrix} -\sin q_l h \\ \cos q_l h \end{pmatrix} \tilde{B}_3 = 0. \quad (44)$$

From Eq. (42) we find that

(A) $k = k_j$, with $k_j a$ as the j th zero of $J'_n(x)$, or $J'_n(k_j a) = 0$ ($j=0, 1, 2, \dots$), including $k_{j=0} = 0$ for $n \geq 0$.

Thus, q_l and q_t are discretized as $q_l = q_{l,j}$ and $q_t = q_{t,j}$ with

$$q_{l,j}^2 + k_j^2 = \omega^2/v_l^2, \quad (45)$$

$$q_{t,j}^2 + k_j^2 = \omega^2/v_t^2. \quad (46)$$

So, for the wave numbers k_j along the radial direction satisfying $k_j^2 > \omega^2/v_l^2$, $q_{l,j}^2$ becomes negative and also for $k_j^2 > \omega^2/v_t^2$, $q_{t,j}^2$ becomes negative. In these cases the lattice displacements are evanescent in the axial direction. Also from Eq. (43)

(B-1) $q = q_m \equiv m\pi/h$ ($m=0, 1, 2, \dots$) for the *even* solution and

(B-2) $q = q_m \equiv (2m+1)\pi/2h$ ($m=0, 1, 2, \dots$) for the *odd* solution.

Thus, k_l and k_t are also discretized as $k_l = k_{l,m}$ and $k_t = k_{t,m}$ with

$$q_m^2 + k_{l,m}^2 = \omega^2/v_l^2, \quad (47)$$

$$q_m^2 + k_{t,m}^2 = \omega^2/v_t^2. \quad (48)$$

Hence, for the wave numbers q_m along the cylindrical axis of the disk satisfying $q_m^2 > \omega^2/v_l^2$, $k_{l,m}^2$ becomes negative and also for $q_m^2 > \omega^2/v_t^2$, $k_{t,m}^2$ becomes negative. In these cases the lattice displacements in the radial direction are described by the modified Bessel function I_n .

We now choose the coefficients of the displacement vector that may satisfy Eqs. (40), (41), and (44). Here we write the coefficients of the displacement vectors as

$$\begin{pmatrix} A_1 \\ A_2 \\ A_3 \end{pmatrix} = \alpha_m \begin{pmatrix} A_{1,m} \\ A_{2,m} \\ A_{3,m} \end{pmatrix}, \quad (49)$$

$$\begin{pmatrix} \tilde{B}_1 \\ \tilde{B}_2 \\ \tilde{B}_3 \end{pmatrix} = \beta_j \begin{pmatrix} \tilde{B}_{1,j} \\ \tilde{B}_{2,j} \\ \tilde{B}_{3,j} \end{pmatrix}, \quad (50)$$

where

$$qk_l J'_n(k_l a) A_{1,m} - \frac{nq}{2a} J_n(k_l a) A_{2,m} + \frac{1}{2} k_l (k_l^2 - q^2) J'_n(k_l a) A_{3,m} = 0, \quad (51)$$

$$\tilde{B}_{1,j} = \frac{1}{2} (k_j^2 - q_{l,j}^2) \begin{pmatrix} -\sin q_{l,j} h \\ \cos q_{l,j} h \end{pmatrix}, \quad (52)$$

$$\tilde{B}_{2,j} = 0, \quad (53)$$

$$\tilde{B}_{3,j} = -q_{l,j} \begin{pmatrix} -\sin q_{l,j}h \\ \cos q_{l,j}h \end{pmatrix}, \quad (54)$$

and (α_m, β_j) are unknown coefficients to be determined. Also, two independent components of the vector \mathbf{A}_m are undetermined. If we set

$$\alpha_m \begin{pmatrix} A_{1,m} \\ A_{2,m} \\ A_{3,m} \end{pmatrix} = \begin{pmatrix} \alpha'_m A'_{1,m} + \gamma_m C_{1,m} \\ \gamma_m C_{2,m} \\ \alpha'_m A'_{3,m} \end{pmatrix}, \quad (55)$$

with

$$A'_{1,m} = \frac{1}{2} k_{l,m} (k_{l,m}^2 - q_m^2) J'_n(k_{l,m}a), \quad (56)$$

$$A'_{3,m} = -q_m k_{l,m} J'_n(k_{l,m}a), \quad (57)$$

$$C_{1,m} = \frac{n}{2a} J_n(k_{l,m}a), \quad (58)$$

$$C_{2,m} = k_{l,m} J'_n(k_{l,m}a), \quad (59)$$

the coefficients $(\alpha'_m, \beta_j, \gamma_m)$ should be determined from remaining boundary conditions. This is a procedure used by Hutchinson,²⁵ but we do not follow this procedure until Sec. V.

With these results the displacement vector $\mathbf{u} = (u_r, u_\theta, u_z)^t$ is written by the superpositions of the terms with different indices m and j , e.g.,

$$u_r(r, \theta, z) = \sum_m \alpha_m [(X_{n,m})_{11} A_{1,m} + (X_{n,m})_{12} A_{2,m} + (X_{n,m})_{13} A_{3,m}] \\ + \sum_j \beta_j [(\tilde{X}_{n,j})_{11} \tilde{B}_{1,j} + (\tilde{X}_{n,j})_{12} \tilde{B}_{2,j} + (X_{n,j})_{13} \tilde{B}_{3,j}], \quad (60)$$

where $(X_{n,m})_{\alpha\beta}$ and $(\tilde{X}_{n,j})_{\alpha\beta}$ are obtained from $(X_n)_{\alpha\beta}$ and $(\tilde{X}_n)_{\alpha\beta}$ by replacing the wave numbers with discretized ones having indices m and j . For $u_\theta(r, \theta, z)$ and $u_z(r, \theta, z)$, we may change $(X_{n,m})_{1i}$ and $(\tilde{X}_{n,j})_{1i}$ to $(X_{n,m})_{2i}$ and $(\tilde{X}_{n,j})_{2i}$, and $(X_{n,m})_{3i}$ and $(\tilde{X}_{n,j})_{3i}$, respectively.

B. Second set of boundary conditions

Next, we consider the remaining boundary conditions

$$T_{rr}(a, \theta, z) = 0, \quad (61)$$

$$T_{r\theta}(a, \theta, z) = 0, \quad (62)$$

$$T_{zz}(r, \theta, \pm h) = 0. \quad (63)$$

The coefficients (α_m, β_j) are determined from these boundary conditions. Explicitly, $T_{rr}(a, \theta, z)$ is written as

$$T_{rr}(a, \theta, z)/2\mu = \sum_m \alpha_m [(S_{n,m}^r)_{11} A_{1,m} + (S_{n,m}^r)_{12} A_{2,m} + (S_{n,m}^r)_{13} A_{3,m}]_{r=a} + \sum_j \beta_j [(\tilde{S}_{n,j}^r)_{11} \tilde{B}_{1,j} + (\tilde{S}_{n,j}^r)_{12} \tilde{B}_{2,j} + (\tilde{S}_{n,j}^r)_{13} \tilde{B}_{3,j}]_{r=a} \\ = \sum_m \alpha_m \left\{ \left[q_m^2 - \frac{\omega^2}{2v_t^2} + \frac{1}{a^2} \chi_n(k_{l,m}a) \right] J_n(k_{l,m}a) A_{1,m} - \frac{n}{a^2} f_n(k_{l,m}a) J_n(k_{l,m}a) A_{2,m} \right. \\ \left. + \frac{q_m}{a^2} [(k_{l,m}a)^2 - \chi_n(k_{l,m}a)] J_n(k_{l,m}a) A_{3,m} \right\} \begin{pmatrix} \cos q_m z \\ \sin q_m z \end{pmatrix} \cos n\theta + \sum_j \beta_j \left\{ \left[q_{l,j}^2 - \frac{\omega^2}{2v_t^2} + \frac{1}{a^2} \chi_n(k_j a) \right] \begin{pmatrix} \cos q_{l,j} z \\ \sin q_{l,j} z \end{pmatrix} \tilde{B}_{1,j} \right. \\ \left. + \frac{q_{l,j}}{a^2} [(k_j a)^2 - \chi_n(k_j a)] \begin{pmatrix} \cos q_{l,j} z \\ \sin q_{l,j} z \end{pmatrix} \tilde{B}_{3,j} \right\} J_n(k_j a) \cos n\theta, \quad (64)$$

where f_n and χ_n are defined in Appendix A. Similarly,

$$T_{r\theta}(a, \theta, z)/2\mu = \sum_m \alpha_m [(S_{n,m}^r)_{21} A_{1,m} + (S_{n,m}^r)_{22} A_{2,m} + (S_{n,m}^r)_{23} A_{3,m}]_{r=a} + \sum_j \beta_j [(\tilde{S}_{n,j}^r)_{21} \tilde{B}_{1,j} + (\tilde{S}_{n,j}^r)_{22} \tilde{B}_{2,j} + (\tilde{S}_{n,j}^r)_{23} \tilde{B}_{3,j}]_{r=a} \\ = \sum_m \alpha_m \left\{ -\frac{n}{a^2} f_n(k_{l,m}a) J_n(k_{l,m}a) A_{1,m} + \frac{1}{a^2} \left[-\frac{1}{2} (k_{l,m}a)^2 + \chi_n(k_{l,m}a) \right] J_n(k_{l,m}a) A_{2,m} + \frac{nq_m}{a^2} f_n(k_{l,m}a) J_n(k_{l,m}a) A_{3,m} \right\} \\ \times \begin{pmatrix} \cos q_m z \\ \sin q_m z \end{pmatrix} \sin n\theta + \sum_j \beta_j \left\{ -\frac{n}{a^2} f_n(k_j a) \begin{pmatrix} \cos q_{l,j} z \\ \sin q_{l,j} z \end{pmatrix} \tilde{B}_{1,j} + \frac{nq_{l,j}}{a^2} f_n(k_j a) \begin{pmatrix} \cos q_{l,j} z \\ \sin q_{l,j} z \end{pmatrix} \tilde{B}_{3,j} \right\} J_n(k_j a) \sin n\theta. \quad (65)$$

The above Eqs. (64) and (65) should be zero irrespective of z in the interval $-h \leq z \leq h$. This can be possible if they are orthogonal to a complete set of functions defined

in the same interval. Such complete sets consist of sinusoidal functions $\{\cos q_m z = \cos(m\pi z/h)\}$ for the even solution and $\{\sin q_m z = \sin[(2m+1)\pi z/2h]\}$ for the odd solution with

$m=0, 1, 2, \dots$ Thus, we require

$$\int_0^h T_{rr}(a, \theta, z) \begin{bmatrix} \cos \frac{m\pi}{h} z \\ \sin \frac{(2m+1)\pi}{2h} z \end{bmatrix} dz = 0, \quad (66)$$

$$\int_0^h T_{r\theta}(a, \theta, z) \begin{bmatrix} \cos \frac{m\pi}{h} z \\ \sin \frac{(2m+1)\pi}{2h} z \end{bmatrix} dz = 0. \quad (67)$$

Accordingly, from Eq. (66) we have

$$\alpha_m \left\{ \left[q_m^2 - \frac{\omega^2}{2v_t^2} + \frac{1}{a^2} \chi_n(k_{l,m}a) \right] J_n(k_{l,m}a) A_{1,m} - \frac{n}{a^2} f_n(k_{t,m}a) J_n(k_{t,m}a) A_{2,m} + \frac{q_m}{a^2} [(k_{t,m}a)^2 - \chi_n(k_{t,m}a)] J_n(k_{t,m}a) A_{3,m} \right\} + \sum_j \beta_j \left\{ \left[q_{t,j}^2 - \frac{\omega^2}{2v_t^2} + \frac{n^2}{a^2} \right] \begin{bmatrix} s_m(q_{l,j}h) \\ c_m(q_{l,j}h) \end{bmatrix} \tilde{B}_{1,j} + \frac{q_{t,j}}{a^2} [(k_j a)^2 - n^2] \begin{bmatrix} s_m(q_{t,j}h) \\ c_m(q_{t,j}h) \end{bmatrix} \tilde{B}_{3,j} \right\} J_n(k_j a) = 0, \quad (68)$$

and from Eq. (67)

$$\alpha_m \left\{ -\frac{n}{a^2} f_n(k_{l,m}a) J_n(k_{l,m}a) A_{1,m} + \frac{1}{a^2} \left[-\frac{1}{2} (k_{t,m}a)^2 + \chi_n(k_{t,m}a) \right] J_n(k_{t,m}a) A_{2,m} + \frac{nq_m}{a^2} f_n(k_{t,m}a) J_n(k_{t,m}a) A_{3,m} \right\} + \sum_j \beta_j \left\{ \frac{n}{a^2} \begin{bmatrix} s_m(q_{l,j}h) \\ c_m(q_{l,j}h) \end{bmatrix} \tilde{B}_{1,j} - \frac{nq_{t,j}}{a^2} \begin{bmatrix} s_m(q_{t,j}h) \\ c_m(q_{t,j}h) \end{bmatrix} \tilde{B}_{3,j} \right\} J_n(k_j a) = 0, \quad (69)$$

where we have used the equations $f_n(k_j a) = -1$ and $\chi_n(k_j a) = n^2$ that hold for k_j satisfying $J'_n(k_j a) = 0$,²⁸ and introduced $s_m(x)$ and $c_m(x)$ defined by

$$s_m(qh) \equiv \frac{2}{h} \int_0^h \cos qz \cos q_m z dz = (-1)^m \frac{2qh}{(qh)^2 - (q_m h)^2} \sin qh \quad (m = 1, 2, \dots), \quad (70)$$

$$c_m(qh) \equiv \frac{2}{h} \int_0^h \sin qz \sin q_m z dz = (-1)^{m+1} \frac{2qh}{(qh)^2 - (q_m h)^2} \cos qh \quad (m = 0, 1, 2, \dots), \quad (71)$$

and

$$s_0(qh) \equiv \frac{1}{h} \int_0^h \cos qz dz = \frac{\sin qh}{qh} \equiv \text{sinc}(qh).$$

Finally, we are left with the boundary condition $T_{zz}(r, \theta, \pm h) = 0$. [$T_{zz}(r, \theta, -h) = 0$ is automatically satisfied if $T_{zz}(r, \theta, h) = 0$.] Explicitly, $T_{zz}(r, \theta, h)$ is

$$T_{zz}(r, \theta, h)/2\mu = \sum_m \alpha_m [(S_{n,m}^z)_{31} A_{1,m} + (S_{n,m}^z)_{32} A_{2,m} + (S_{n,m}^z)_{33} A_{3,m}]_{z=h} + \sum_j \beta_j [(\tilde{S}_{n,j}^z)_{31} \tilde{B}_{1,j} + (\tilde{S}_{n,j}^z)_{32} \tilde{B}_{2,j} + (\tilde{S}_{n,j}^z)_{33} \tilde{B}_{3,j}]_{z=h} = \sum_m \alpha_m (-1)^m \left[\left(k_{l,m}^2 - \frac{\omega^2}{2v_t^2} \right) J_n(k_{l,m}r) A_{1,m} - q_m k_{t,m}^2 J_n(k_{t,m}r) A_{3,m} \right] \cos n\theta + \sum_j \beta_j \left[\frac{1}{2} (k_j^2 - q_{t,j}^2) \tilde{B}_{1,j} \begin{pmatrix} \cos q_{l,j}h \\ \sin q_{l,j}h \end{pmatrix} - q_{t,j} k_j^2 \begin{pmatrix} \cos q_{t,j}h \\ \sin q_{t,j}h \end{pmatrix} \tilde{B}_{3,j} \right] J_n(k_j r) \cos n\theta. \quad (72)$$

This equation should also be zero identically. This is possible if Eq. (72) is orthogonal to the functions forming a complete set in the interval $0 \leq r \leq a$. We choose the functions $\{J_n(k_j r)\}$ with $J'_n(k_j a) = 0$ as the complete set in this interval and require

$$\int_0^a T_{zz}(r, \theta, h) J_n(k_j r) r dr = 0 \quad (j = 1, 2, 3, \dots). \quad (73)$$

Here we note that $T_{zz}(r, \theta, h)$ involves $J_n(kr)$ [and possibly

$J_n(i\kappa a) = i^n I_n(\kappa a)$] but not its derivative $J'_n(kr)$. Hence, to evaluate the integral of Eq. (73), we can use the equation²⁹

$$\int_0^a J_n(kr)J_n(k_j r) r dr = \frac{ka}{k_j^2 - k^2} J'_n(ka)J_n(k_j a) \quad (74)$$

and the orthogonality of the Bessel functions

$$\int_0^a J_n(k_j r)J_n(k_j' r) r dr = \delta_{jj'} \frac{a^2}{2} \left[1 - \frac{n^2}{(k_j a)^2} \right] [J_n(k_j a)]^2, \quad (75)$$

for $J'_n(k_j a) = J'_n(k_j' a) = 0$. Thus, we find from Eq. (73)

$$\begin{aligned} \sum_m \alpha_m (-1)^m \left[\left(2k_{l,m}^2 - \frac{\omega^2}{v_t^2} \right) \frac{k_{l,m} a}{(k_j a)^2 - (k_{l,m} a)^2} J'_n(k_{l,m} a) A_{1,m} \right. \\ \left. - q_m k_{l,m}^2 \frac{k_{l,m} a}{(k_j a)^2 - (k_{l,m} a)^2} J'_n(k_{l,m} a) A_{3,m} \right] \\ + \beta_j \left[\frac{1}{2} (k_j^2 - q_{t,j}^2) \begin{pmatrix} \cos q_{l,j} h \\ \sin q_{l,j} h \end{pmatrix} \tilde{B}_{1,j} - q_{t,j} k_j^2 \begin{pmatrix} \cos q_{t,j} h \\ \sin q_{t,j} h \end{pmatrix} \tilde{B}_{3,j} \right] \\ \times \left[1 - \frac{n^2}{(k_j a)^2} \right] J_n(k_j a) = 0, \quad (76) \end{aligned}$$

where $a^2 J_n(k_j a)/2$ has been factored out from the left-hand side of Eq. (76). Thus Eqs. (68), (69), and (76) constitute the equations for determining the coefficients (α_m, β_j) as well as the eigenfrequencies of the disk.

IV. DETERMINATION OF EIGENFREQUENCIES

A. Equations for the eigenfrequencies

To solve Eqs. (68), (69), and (76), it is convenient to decompose $\{\alpha_m\}$ into $\{\alpha'_m\}$ and $\{\gamma_m\}$ according to Eqs. (55)–(59). We also have to truncate the expansions over m and j with N_z and N_r terms, respectively. Hence, introducing N_z component vectors $\boldsymbol{\alpha}' = (\alpha'_1, \alpha'_2, \dots, \alpha'_{N_z})^t$ and $\boldsymbol{\gamma} = (\gamma_1, \gamma_2, \dots, \gamma_{N_z})^t$ and an N_r component vector $\boldsymbol{\beta} = (\beta_1, \beta_2, \dots, \beta_{N_r})^t$ consisting of undetermined coefficients, Eqs. (68), (69), and (76) deduced from the boundary conditions are summarized as

$$M_A^{(1)} \boldsymbol{\alpha}' + M_B^{(1)} \boldsymbol{\beta} + M_C^{(1)} \boldsymbol{\gamma} = 0, \quad (77)$$

$$M_A^{(2)} \boldsymbol{\alpha}' + M_B^{(2)} \boldsymbol{\beta} + M_C^{(2)} \boldsymbol{\gamma} = 0, \quad (78)$$

$$M_A^{(3)} \boldsymbol{\alpha}' + M_B^{(3)} \boldsymbol{\beta} + M_C^{(3)} \boldsymbol{\gamma} = 0, \quad (79)$$

where Eqs. (77)–(79) are originated from $T_{rr}(a, \theta, z) = 0$, $T_{zz}(r, \theta, \pm h) = 0$, and $T_{r\theta}(a, \theta, z) = 0$, respectively.

Accordingly, $(2N_z + N_r)$ eigenfrequencies of the vibrational modes are determined by solving the equation

$$\det \begin{pmatrix} M_A^{(1)} & M_B^{(1)} & M_C^{(1)} \\ M_A^{(2)} & M_B^{(2)} & M_C^{(2)} \\ M_A^{(3)} & M_B^{(3)} & M_C^{(3)} \end{pmatrix} = 0, \quad (80)$$

where $N_z \times N_z$ -diagonal matrices $M_A^{(1)}$, $M_A^{(3)}$, $M_C^{(1)}$, and $M_C^{(3)}$,

and $N_r \times N_r$ -diagonal matrix $M_B^{(2)}$ are given by

$$\begin{aligned} [M_A^{(1)}]_{mm} = \frac{1}{2a^3} (k_{t,m}^2 - q_m^2) \left[(q_m a)^2 - \frac{1}{2} \left(\frac{\omega a}{v_t} \right)^2 + \chi_n(k_{l,m} a) \right] \\ \times J_n(k_{l,m} a) (k_{l,m} a) J'_n(k_{l,m} a) \\ + \frac{q_m^2}{a^3} [-(k_{l,m} a)^2 + \chi_n(k_{l,m} a)] J_n(k_{l,m} a) \\ \times (k_{l,m} a) J'_n(k_{l,m} a), \quad (81) \end{aligned}$$

$$\begin{aligned} [M_C^{(1)}]_{mm} = \frac{n}{2a^3} \left\{ \left[(q_m a)^2 - \frac{1}{2} \left(\frac{\omega a}{v_t} \right)^2 + \chi_n(k_{l,m} a) \right] J_n(k_{l,m} a) \right. \\ \left. - 2f_n(k_{l,m} a) (k_{l,m} a) J'_n(k_{l,m} a) \right\} J_n(k_{l,m} a), \quad (82) \end{aligned}$$

$$\begin{aligned} [M_A^{(3)}]_{mm} = -\frac{n}{2a^3} [(k_{t,m}^2 - q_m^2) f_n(k_{l,m} a) J_n(k_{l,m} a) (k_{l,m} a) J'_n(k_{l,m} a) \\ + 2q_m^2 f_n(k_{l,m} a) J_n(k_{l,m} a) (k_{l,m} a) J'_n(k_{l,m} a)], \quad (83) \end{aligned}$$

$$\begin{aligned} [M_C^{(3)}]_{mm} = \frac{1}{a^3} \left\{ -\frac{n^2}{2} f_n(k_{l,m} a) J_n(k_{l,m} a) \right. \\ \left. + \left[-\frac{1}{2} (k_{l,m} a)^2 + \chi_n(k_{l,m} a) \right] \right. \\ \left. \times (k_{l,m} a) J'_n(k_{l,m} a) \right\} J_n(k_{l,m} a), \quad (84) \end{aligned}$$

$$\begin{aligned} [M_B^{(2)}]_{jj} = \left[\frac{1}{4} (k_j^2 - q_{t,j}^2)^2 \begin{pmatrix} -q_{t,j} h \cos q_{l,j} h \operatorname{sinc}(q_{t,j} h) \\ q_{l,j} h \cos q_{t,j} h \operatorname{sinc}(q_{l,j} h) \end{pmatrix} \right. \\ \left. + \frac{k_j^2}{h^2} \begin{pmatrix} -q_{t,j} h (q_{l,j} h)^2 \cos q_{t,j} h \operatorname{sinc}(q_{l,j} h) \\ q_{l,j} h (q_{t,j} h)^2 \cos q_{l,j} h \operatorname{sinc}(q_{t,j} h) \end{pmatrix} \right] \\ \times \left[1 - \frac{n^2}{(k_j a)^2} \right] J_n(k_j a). \quad (85) \end{aligned}$$

Also $N_z \times N_r$ matrices $M_B^{(1)}$ and $M_B^{(3)}$, and $N_r \times N_z$ matrices $M_A^{(2)}$ and $M_C^{(2)}$ are given by

$$\begin{aligned} [M_B^{(1)}]_{mj} = \frac{(-1)^{m+1}}{(ha)^2} (q_{l,j} h) \\ \times \left\{ \frac{k_j^2 - q_{t,j}^2}{q_{l,j}^2 - q_m^2} \left[(q_{l,j} a)^2 - \frac{1}{2} \left(\frac{\omega a}{v_t} \right)^2 + n^2 \right] \right. \\ \left. + \frac{2q_{t,j}^2}{q_{t,j}^2 - q_m^2} [n^2 - (k_j a)^2] \right\} \\ \times \left[\frac{(q_{l,j} h) (q_{t,j} h) \operatorname{sinc}(q_{l,j} h) \operatorname{sinc}(q_{t,j} h)}{\cos(q_{l,j} h) \cos(q_{t,j} h)} \right] J_n(k_j a), \quad (86) \end{aligned}$$

$$[M_B^{(3)}]_{mj} = \frac{(-1)^{m+1}}{(ha)^2} n(q_{l,j}h) \left(\frac{k_j^2 - q_{t,i}^2}{q_{l,j}^2 - q_m^2} + \frac{2q_{t,j}^2}{q_{t,j}^2 - q_m^2} \right) \times \left[\frac{(q_{l,j}h)(q_{t,j}h) \operatorname{sinc}(q_{l,j}h) \operatorname{sinc}(q_{t,j}h)}{\cos(q_{l,j}h) \cos(q_{t,j}h)} \right] J_n(k_j a), \quad (87)$$

$$[M_A^{(2)}]_{jm} = \frac{(-1)^m}{a^3} \left[\frac{k_{t,m}^2 - q_m^2}{k_j^2 - k_{l,m}^2} \left(k_{l,m}^2 - \frac{\omega^2}{2v_t^2} \right) + \frac{2q_m^2 k_{t,m}^2}{k_j^2 - k_{l,m}^2} \right] \times (k_{l,m} a) J'_n(k_{l,m} a) (k_{t,m} a) J'_n(k_{t,m} a), \quad (88)$$

$$[M_C^{(2)}]_{jm} = \frac{(-1)^m}{a^3} \frac{n}{k_j^2 - k_{l,m}^2} \left(k_{l,m}^2 - \frac{\omega^2}{2v_t^2} \right) \times (k_{l,m} a) J'_n(k_{l,m} a) J_n(k_{t,m} a). \quad (89)$$

Because the matrices $M_A^{(1)}$, $M_A^{(3)}$, $M_C^{(1)}$, $M_C^{(3)}$, and $M_B^{(2)}$ are diagonal, the condensation of the $(2N_z + N_r) \times (2N_z + N_r)$ matrix in Eq. (80) composed of the coefficients of Eqs. (77)–(79) into a $N_r \times N_r$ matrix is possible only with trivial inversion of diagonal matrices.

B. Displacement vectors

Once an eigenfrequency of the disk is obtained, the components of the corresponding lattice displacement are calculated from the equations

$$u_r(r, \theta, z) / \cos n\theta = \sum_m \frac{\alpha'_m}{a^2} \left[\frac{1}{2} (k_{t,m}^2 - q_m^2) \frac{J'_n(k_{t,m} a)}{(k_{t,m} a)^{n-1}} \frac{J'_n(k_{l,m} r)}{(k_{l,m} a)^{n-1}} + q_m^2 \frac{J'_n(k_{l,m} a)}{(k_{l,m} a)^{n-1}} \frac{J'_n(k_{t,m} r)}{(k_{t,m} a)^{n-1}} \right] (\cos q_m z) + \sum_j \beta_j k_j \left[\frac{1}{2} (k_j^2 - q_{t,j}^2) \left(\frac{z}{h} \cos q_{t,j} h \operatorname{sinc} q_{l,j} z \right) + \left(\frac{q_{l,j}^2 \operatorname{sinc} q_{l,j} h \cos q_{t,j} z}{\frac{z}{h} q_{t,j}^2 \cos q_{l,j} h \operatorname{sinc} q_{t,j} z} \right) \right] \frac{J'_n(k_j r)}{J_n(k_j a)} + \sum_m \gamma_m \frac{n}{a^2} \left[\frac{1}{2} \frac{J_n(k_{t,m} a)}{(k_{t,m} a)^n} \frac{J'_n(k_{l,m} r)}{(k_{l,m} a)^{n-1}} - \frac{a}{r} \frac{J'_n(k_{l,m} a)}{(k_{l,m} a)^{n-1}} \frac{J_n(k_{t,m} r)}{(k_{t,m} a)^n} \right] (\cos q_m z), \quad (90)$$

$$u_\theta(r, \theta, z) / \sin n\theta = \sum_m \alpha'_m \left(-\frac{n}{ar} \right) \left[\frac{1}{2} (k_{t,m}^2 - q_m^2) \frac{J'_n(k_{t,m} a)}{(k_{t,m} a)^{n-1}} \frac{J_n(k_{l,m} r)}{(k_{l,m} a)^n} + q_m^2 \frac{J'_n(k_{l,m} a)}{(k_{l,m} a)^{n-1}} \frac{J_n(k_{t,m} r)}{(k_{t,m} a)^n} \right] (\cos q_m z) + \sum_j \beta_j \left(-\frac{n}{r} \right) \left[\frac{1}{2} (k_j^2 - q_{t,j}^2) \left(\frac{z}{h} \cos q_{t,j} h \operatorname{sinc} q_{l,j} z \right) + \left(\frac{q_{l,j}^2 \operatorname{sinc} q_{l,j} h \cos q_{t,j} z}{\frac{z}{h} q_{t,j}^2 \cos q_{l,j} h \operatorname{sinc} q_{t,j} z} \right) \right] \frac{J_n(k_j r)}{J_n(k_j a)} + \sum_m \gamma_m \frac{1}{a^2} \left[-\frac{n^2 a}{2 r} \frac{J_n(k_{t,m} a)}{(k_{t,m} a)^n} \frac{J_n(k_{l,m} r)}{(k_{l,m} a)^n} + \frac{J'_n(k_{l,m} a)}{(k_{l,m} a)^{n-1}} \frac{J'_n(k_{t,m} r)}{(k_{t,m} a)^{n-1}} \right] (\cos q_m z), \quad (91)$$

$$u_z(r, \theta, z) / \cos n\theta = \sum_m \alpha'_m \frac{q_m}{a} \left[\frac{1}{2} (k_{t,m}^2 - q_m^2) \frac{J'_n(k_{t,m} a)}{(k_{t,m} a)^{n-1}} \frac{J_n(k_{l,m} r)}{(k_{l,m} a)^n} - k_{t,m}^2 \frac{J'_n(k_{l,m} a)}{(k_{l,m} a)^{n-1}} \frac{J_n(k_{t,m} r)}{(k_{t,m} a)^n} \right] (-\sin q_m z) + \sum_j \beta_j \left[\frac{1}{2} (k_j^2 - q_{t,j}^2) \left(-\frac{q_{l,j}^2 z \operatorname{sinc} q_{t,j} h \operatorname{sinc} q_{l,j} z}{\frac{1}{h} \cos q_{t,j} h \cos q_{l,j} z} \right) - k_j^2 \left(-\frac{q_{l,j}^2 \operatorname{sinc} q_{l,j} h \operatorname{sinc} q_{t,j} z}{\frac{1}{h} \cos q_{l,j} h \cos q_{t,j} z} \right) \right] \frac{J_n(k_j r)}{J_n(k_j a)} + \sum_m \gamma_m \frac{n}{2a} q_m \frac{J_n(k_{t,m} a)}{(k_{t,m} a)^n} \frac{J_n(k_{l,m} r)}{(k_{l,m} a)^n} (-\sin q_m z). \quad (92)$$

V. NUMERICAL EXAMPLES

Based on the above formulations we will develop numerical examples for the vibrational properties of a free cylindrical disk (radius a and thickness $2h$) by assuming a polycrystalline aluminum which is elastically isotropic. The mass

density and the longitudinal and transverse sound velocities used for the numerical calculations are $\rho = 2.73 \text{ g cm}^{-3}$, $v_l = 6.37 \times 10^5 \text{ cm/s}$, and $v_t = 3.09 \times 10^5 \text{ cm/s}$, respectively. The ratio v_l/v_t is 2.06 for aluminum. It is convenient to normalize the vibrational frequency ω by multiplying the radius a and dividing by v_t . Then, the lowest normalized

frequency $\omega a/v_t$ of the disk (with $h \sim a$) for a given angular wave number n (equivalent to the order of the Bessel function) is roughly equal to n . This is because the boundary conditions in the radial direction lead approximately to $J'_n(ka) = J'_n(\omega a/v_t) = 0$ and the smallest (but finite) zero of $J'_n(x)$ cannot be less than n .³⁰ (More details will be given below.) Hence, typically $\omega \sim nv_t/a = 3.09 \times n$ GHz (THz) for a microdisk (nanodisk) with $a = 1 \mu\text{m}$ (nm).

A. Axisymmetric ($n=0$) modes

Before starting the numerical analysis of the vibrational modes with a finite angular wave number n , we briefly recapitulate the axisymmetric modes (independent of θ) with $n=0$ because some of their characteristics are often found in the case of $n \neq 0$. First we note that by setting $n=0$ in Eq. (14), the displacements (u_r, u_z) in the r - z plane are decoupled from u_θ governing the torsional motion of the cylinder. Although it is not possible to give a simple closed form expression for the eigenfrequencies of the coupled (u_r, u_z) modes, analytic solutions for the vibrational spectra of the torsional mode are readily obtained for $n=0$. The lattice displacement of this mode is deduced from the potential $\phi_{j=2}$ and by interchanging $\sin \theta$ and $\cos \theta$ in Eqs. (10) and (15). Explicitly, the only nonzero element of the lattice displacement of Eq. (15), i.e., $[X_0(r, \theta, z)]_{22}$, for this mode gives

$$\begin{aligned} u_\theta(r, \theta, z) &= u_\theta(r, z) \\ &= A_2 k_r J'_0(k_r r) \begin{pmatrix} \cos qz \\ \sin qz \end{pmatrix} e^{-i\omega t} \\ &= -A_2 k_r J_1(k_r r) \begin{pmatrix} \cos qz \\ \sin qz \end{pmatrix} e^{-i\omega t}. \end{aligned} \quad (93)$$

The associated stresses are

$$T_{r\theta}(r, z)/\mu = A_2 k_r^2 J_2(k_r r) \begin{pmatrix} \cos qz \\ \sin qz \end{pmatrix} e^{-i\omega t}, \quad (94)$$

$$T_{z\theta}(r, z)/\mu = -A_2 q k_r J_1(k_r r) \begin{pmatrix} -\sin qz \\ \cos qz \end{pmatrix} e^{-i\omega t}. \quad (95)$$

From the stress-free boundary conditions $T_{r\theta}(a, z) = T_{z\theta}(r, \pm h) = 0$, we have

$$J_2(k_r a) = 0, \quad (96)$$

$$\begin{pmatrix} \sin qh \\ \cos qh \end{pmatrix} = 0. \quad (97)$$

Thus, the eigenfrequencies are discretized as $\omega = v_t \sqrt{k_r^2 + q^2} \equiv \omega_{j,m}$, where

$$\frac{\omega_{j,m} a}{v_t} = [(k_j a)^2 + (q_m a)^2]^{1/2} = \left[(k_j a)^2 + \left(\frac{m\pi}{2h/a} \right)^2 \right]^{1/2}, \quad (98)$$

with $k_j a = k_j a$ ($j=0, 1, 2, \dots$) as the zeros of the Bessel function, i.e., $J_2(k_j a) = 0$ [explicitly, $k_0 a = 0$, $k_1 a = 5.136$, $k_2 a = 8.417$, and $k_j a \approx (4j+3)\pi/4$ for large j]. Also,

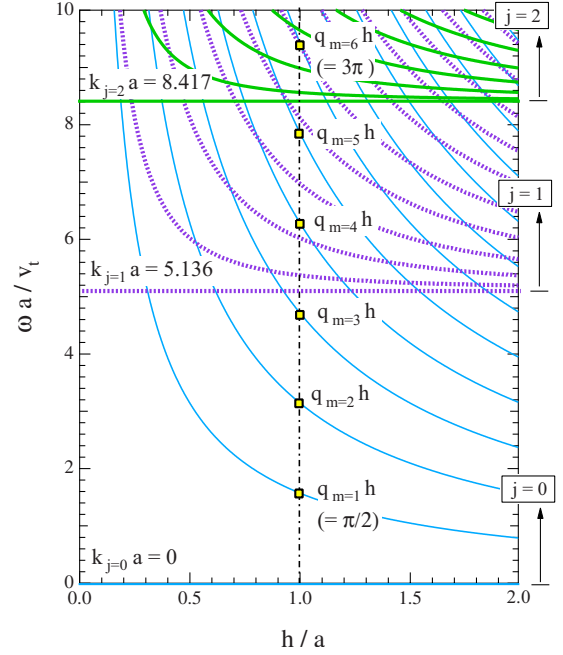


FIG. 1. (Color online) Normalized frequencies versus aspect ratio h/a (≤ 2) of the cylindrical disk for the torsional mode with $n=0$ [Eq. (98)]. Thin solid, dotted, and bold solid lines are the branches with $j=0$, $j=1$, and $j=2$, respectively. Horizontal lines indicate the frequencies $\omega a/v_t = k_j a$ ($j=0, 1, 2$) satisfying $J_2(k_j a) = 0$.

$q = q_m = m\pi/2h$, with $m=0, 2, 4, \dots$ for the even solutions and $m=1, 3, 5, \dots$ for the odd solutions. For $k_r = k_0 = 0$, $u_\theta(r, z)$ is identically zero but we can find another solution,³¹

$$u_\theta(r, z) \propto r \begin{pmatrix} \cos qz \\ \sin qz \end{pmatrix} e^{-i\omega t}, \quad (99)$$

for which the eigenfrequencies are given by $\omega = \omega_{0,m}$ with $\omega_{0,m} a/v_t = m\pi/(2h/a)$. Setting $m=0$, we have $\omega_{0,m=0} = 0$ and this corresponds to the rigid rotation.

As shown in Fig. 1, the spectra consist of the families of branches that approach $k_j a$ for $h/a \rightarrow \infty$. Several features similar to these characteristics of the torsional frequencies will be also seen for $n \neq 0$.

B. Comparison with the resonant ultrasound spectroscopy calculation for small angular wave numbers n

Our formulation for the vibrational frequencies is based on the ones developed by Rasband²¹ and Hutchinson.²⁵ Unfortunately, no numerical result was given by the former. The validity of the formulas obtained by Hutchinson has been confirmed by the comparison with the experimental frequencies measured by McMahon³² for $n \leq 3$ and for certain restricted regions in the $\omega a/v_t$ versus h/a plane. Here, in order to check the reliability of our computer codes, we compare in Fig. 2 the eigenfrequencies of the even and odd solutions (for small angular wave numbers $n \leq 6$) with those obtained by a basis function method sometimes called RUS method.²² In these calculations we have kept $N_r = 3$ and $N_z \sim (h/a)N_r = 3(h/a)$ terms in the sums over m and j , as suggested by

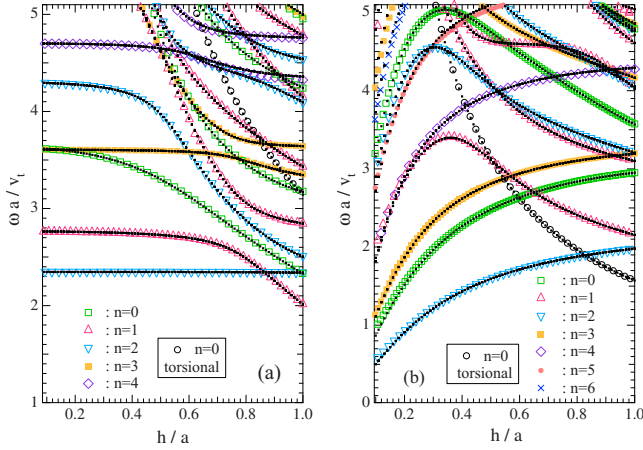


FIG. 2. (Color online) Normalized frequency $\omega a/v_l$ (for $\omega a/v_l < 5$) versus aspect ratio h/a (for $h/a < 1$) of (a) even solutions and (b) odd solutions with small angular wave numbers $n=0-6$ as shown by circles (the torsional mode with $n=0$), open squares (the coupled longitudinal and transverse modes with $n=0$), triangles ($n=1$), inverted triangles ($n=2$), filled squares ($n=3$), diamonds ($n=4$), filled circles ($n=5$), and crosses ($n=6$). Small black dots are the results of the resonant ultrasound spectroscopy (RUS) calculation obtained with 285×285 matrices.

Hutchinson.²⁵ However, $N_r=5-10$ are necessary in order to achieve quantitative coincidence for the odd solutions with $n \leq 3$ in the region of small aspect ratio $h/a < 0.2$. Here we again stress that the rank of the matrix for which we have to find the zeros of the determinant is just N_r , as remarked at the end of Sec. IV A.

The advantage of the RUS method originates in the fact that the displacement vector \mathbf{u} satisfying the equations of motion in the lattice together with the stress-free boundary conditions at sample surfaces gives an extremum of the Lagrangian of the system. In this scheme we start from expanding \mathbf{u} in terms of a set of basis functions, for example, of the form of $x^m y^n z^k$ (called the *xyz* algorithm with non-negative integers m , n , and k) with which the integration of the Lagrangian density over the volume of the medium may be readily carried out. The condition that the Lagrangian is stationary under the variation in \mathbf{u} is then attained by setting the derivatives of the Lagrangian with respect to the expansion coefficients equal to zero. This leads to a generalized eigenvalue equation that determines the resonant frequencies of an elastic body.

In applying this algorithm to the present problem, we need to modify the scheme a bit. Explicitly, for the *even* solution we may expand the displacement vector \mathbf{u} as

$$u_x = \sum_{\lambda} a_{x,\lambda} x^m y^n z^{2l}, \quad (100)$$

$$u_y = \sum_{\lambda} a_{y,\lambda} x^m y^n z^{2l}, \quad (101)$$

$$u_z = \sum_{\nu} a_{z,\nu} x^m y^n z^{2l+1}, \quad (102)$$

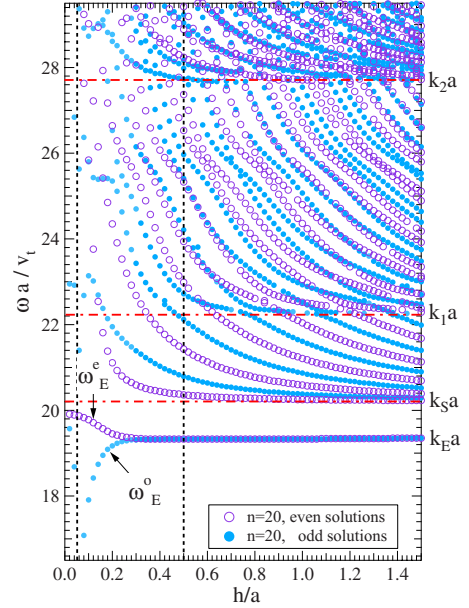


FIG. 3. (Color online) The normalized frequency $\omega a/v_l$ versus aspect ratio h/a (< 1.5) for the angular wave number $n=20$. Open circles and dots show the even and odd solutions, respectively. The horizontal dot-dashed line denoted by $k_{S^*} a (= \omega_{S^*} a/v_l) = 20.21$ is the normalized surface-mode frequency in the cylinder of infinite length. Those by $k_1 a = 22.22$ and $k_2 a = 27.71$ are the lowest two (finite) zeros of $J'_{n=20}(ka)$. Also $k_E a (= \omega_E a/v_l) = 19.38$ is the edge-mode frequency. The vertical dashed lines indicate the positions of $h/a = 0.05$ and 0.5 .

where $\lambda = (m, n, 2l)$ and $\nu = (m, n, 2l+1)$. (For the *odd* solution we may use a similar expansion but with $2l$ and $2l+1$ interchanged.) The rank R of the matrix to be diagonalized is determined by restricting non-negative integers m , n , and l , for instance, to $m+n+2l \leq 2N$. In this case we find $R = (N+1)(N+2)(4N+3)/2$.

The comparison of the resonant frequencies with $N=4$ ($R=285$) is illustrated in Fig. 2 for both the even and odd solutions. The coincidence of our results with the ones obtained by the RUS method is excellent in the range of $\omega a/v_l$ and h/a displayed. (At very small $h/a < 0.1$, the comparison is messy because a number of frequencies belonging to the branches with $n > 6$ are present densely for the odd solutions.) Here we also note the fact that even with such a large matrix with $R \sim 300$, the convergence of the frequencies in the RUS method is not very well in the range $\omega a/v_l > 5$.

C. Edge modes and surface modes for a large angular wave number n

Figure 3 exhibits for a large angular wave number, $n=20$, the eigenfrequencies versus aspect ratio h/a of the cylindrical disk. This result has been calculated with $N_r=N_z=5$ for $h/a \leq 0.3$ and $N_r=5$ and $N_z=20$ for $0.3 < h/a < 1.5$. Here we note that only five terms of the Bessel functions are used in the expansion of lattice displacements over j [Eqs. (90)–(92)] in the radial direction. This leads to a well-converged result for the eigenfrequencies in the range illustrated, i.e., $\omega a/v_l < 30$ (see also Fig. 4). How-

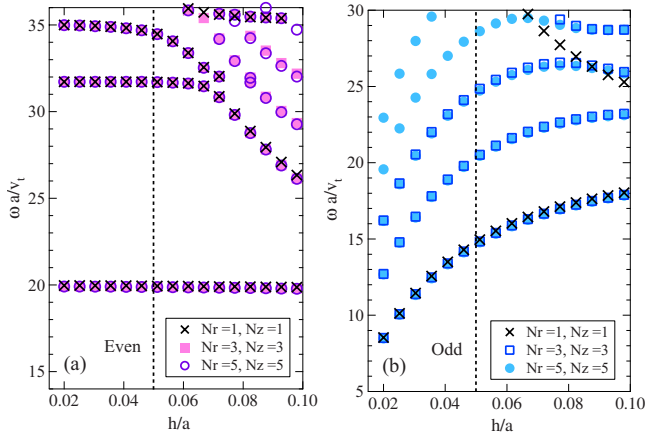


FIG. 4. (Color online) Normalized frequency $\omega a/v_t$ in the small h/a regions ($h/a=0.02-0.1$) for the angular wave number $n=20$. (a) Even solutions and (b) odd solutions. Crosses, squares, and circles are the frequencies obtained by keeping the terms $(N_r, N_z)=(1, 1)$, $(3, 3)$, and $(5, 5)$ in Eq. (80). The vertical dashed lines indicate the positions of $h/a=0.05$.

ever, in order to achieve a good convergence when we increase the ratio h/a , the number of the sinusoidal functions in the axial direction (the sum over m) needs to be increased, in particular for the lowest branch. Thus, in Fig. 3, $N_z=20$ much larger than $N_r=5$ has been assumed for the range of the aspect ratio $h/a=0.3-1.5$.

Interestingly, for small h/a (for instance, $h/a=0.02-0.1$ as illustrated in Fig. 4) we see that the smallest number of terms ($N_r=N_z=1$) are enough to determine the frequencies in the lowest branch for both the even and odd solutions. Hence, as far as the resonant frequencies of the lowest couple of branches (in which we are interested) are concerned, $N_r=N_z=3$ are sufficient to obtain the accurate results in a good approximation, though we sometimes keep more terms in the expansion.

The distribution of eigenfrequencies shown in Fig. 3 is qualitatively the same for the angular wave numbers $n > 5$. More precisely, we can recognize the following characteristic features in common:

(1) The existence of the lowest two branches that are well separated from upper branches. The eigenfrequencies of these branches, which we denote by ω_E^e and ω_E^o for the even and odd solutions, respectively, become degenerate as h/a increases and independent of the thickness ($2h$) of the disk typically in the range of $h/a > 0.5$. Here we define their limiting frequency $\omega = \omega_E \equiv k_E v_t$ for large h , i.e., $\omega_E^e = \omega_E^o = \omega_E$ for $h \rightarrow \infty$, where ω_E depends on the angular wave number n . As we shall see below, the vibrational amplitudes associated with these lowest branches are well localized at the edges between the sidewall and the end planes of the disk. Thus, we call the vibrations in these branches as the *edge modes* and ω_E as the edge-mode frequency.

The dependence of ω_E^e and ω_E^o on the angular wave number n is summarized in Fig. 5 for the disks with $h/a=0.5$ and 1. For large n (>10) the degeneracy of ω_E^e and ω_E^o is clearly seen for these values of the aspect ratios h/a because the vibrational amplitudes are well trapped at the edges as shown in Figs. 6 and 7. For small n , however, the vibrational am-

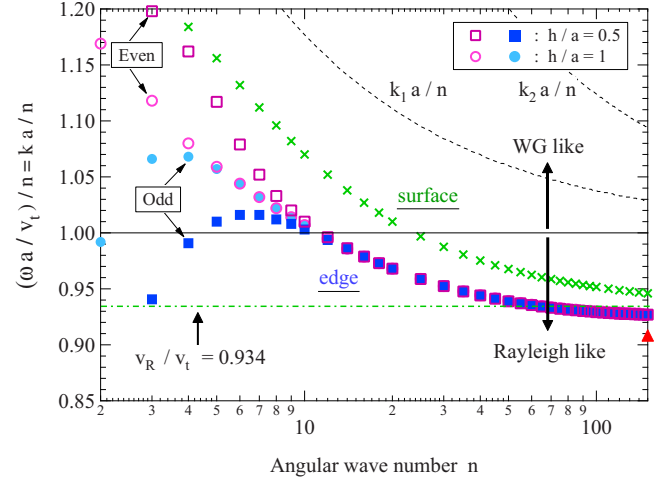
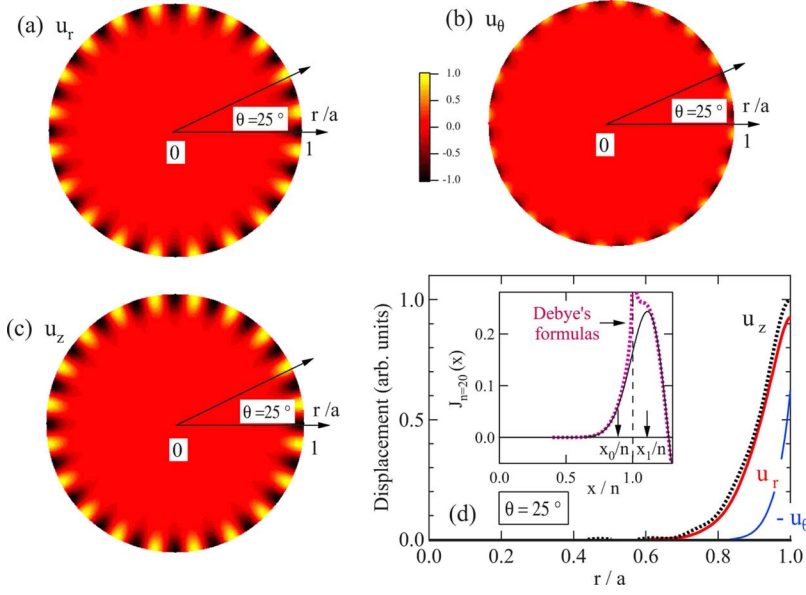


FIG. 5. (Color online) Normalized frequencies (divided by angular wave number) versus angular wave number n in cylindrical disks. Open and filled circles are the *even* and *odd* solutions of the edge modes for $h=a$. The same results for $h=a/2$ are shown by open and filled squares. (The triangle shows the frequency of the lowest edge mode at a right-angle wedge.) Crosses are the surface-mode frequencies in the infinitely long cylinder [obtained from Eq. (107)] normalized by n and equivalent to the ratios of the surface-wave velocity v_S to the velocity v_t of the bulk transverse sound. The horizontal dot-dashed line indicates the same ratio on the flat surface, $v_R/v_t=0.934$, i.e., the Rayleigh wave velocity v_R to v_t . The dashed lines are the smallest (nonzero) two zeros $k_1 a$ and $k_2 a$ (divided by n) of $J'_n(ka)$.

plitudes extend from the edges toward the center $r=0$ of the circular plane. More importantly, they also extend along the cylindrical axis toward halfway of the thickness $z=0$ (see Sec. V D for details). Thus, the lattice displacements are finite and overlapped around $z=0$ and $r=a$, leading to the separation of ω_E^e and ω_E^o of the even and odd solutions. This can be seen for $n < 10$ in the disk with $h/a=0.5$. This separation of resonant frequencies is, however, much smaller for the thicker disk with $h/a=1$ as expected, and recognizable only for $n \leq 4$.

The formulation for the frequencies of long-wavelength edge modes localized at a right-angle elastic wedge occupying the quadrant $x, z \geq 0$, $-\infty \leq y \leq \infty$ (corresponding to the case of $a, h \rightarrow \infty$) was developed by Maradudin *et al.*³³ They solved the equations of motion for the lattice by expanding the displacement vectors in a double series of Laguerre functions that are orthonormal and complete in the space $x, z \geq 0$. Applying their formulas, we find the lowest frequency with which we identify ω_E for $n \rightarrow \infty$ as $\omega_E a/v_t = k_E a = 0.9067 \times n$ for aluminum (the triangle in Fig. 5). This is consistent with the numerical results of the edge-mode frequencies at large n shown in Fig. 5.

(2) Except for very thin disks, the eigenfrequencies of the branches situated above the edge modes decrease as h/a increases (typically for $h/a > 0.2$). Moreover as seen in Fig. 3, in the limit of large h/a , they approach the characteristic frequencies $\omega_j a/v_t = k_j a$ ($j=1, 2, \dots$), determined from the equation $J'_n(\omega_j a/v_t) = J'_n(k_j a) = 0$. These behaviors in $\omega a/v_t$ versus h/a are similar to the torsional modes (with $n=0$) shown in Fig. 1. Here we note that for large n , the smallest two zeros of $J'_n(x)$, or extrema of $J_n(x)$, are³⁴



$$x_1 = k_1 a \sim n + 0.8086n^{1/3} + 0.07n^{-1/3} + o(n^{-4/3}), \quad (103)$$

$$x_2 = k_2 a \sim n + 2.578n^{1/3} + 1.95n^{-1/3} + o(n^{-4/3}). \quad (104)$$

These formulas give $k_1 a = 22.22$ (22.22) and $k_2 a = 27.72$ (27.71) for $n=20$, which are in good coincidence with the locations indicated in Fig. 3 and also the exact zeros given in the parentheses.

(3) For $h/a \rightarrow \infty$ the frequencies in the second lowest branches of the disk (both the even and odd solutions) converge to the frequency $\omega = \omega_S \equiv k_S v_t$ of the Rayleigh-type surface waves on the *curved* surface of an *infinitely long* cylinder. This frequency ω_S (also depending on n) can be derived in our formulation as follows. First we note that relevant boundary conditions for this case are $T_{rr}(a, \theta, z) = 0$ and $T_{r\theta}(a, \theta, z) = 0$, and they lead to

$$\det \begin{pmatrix} M_A^{(1)} & M_C^{(1)} \\ M_A^{(3)} & M_C^{(3)} \end{pmatrix} = 0, \quad (105)$$

where $M_A^{(1)}$, $M_A^{(3)}$, $M_C^{(1)}$, and $M_C^{(3)}$ are the scalar quantities obtained by setting $q_m = 0$ in Eqs. (81)–(84) and also by changing $k_{l,m} \rightarrow k_l = \omega/v_l$ and $k_{t,m} \rightarrow k_t = \omega/v_t$. Explicitly, Eq. (105) gives

$$\left[\chi_n(k_t a) - \frac{1}{2}(k_t a)^2 \right] \left[\chi_n(k_r a) - \frac{1}{2}(k_r a)^2 \right] - n^2 f_n(k_t a) f_n(k_r a) = 0. \quad (106)$$

This equation is equivalent to¹⁵

$$\left[J_{n+2}(k_l a) + J_{n-2}(k_l a) - 2 \left(\frac{v_l^2}{v_t^2} - 1 \right) J_n(k_l a) \right] \times [J_{n+2}(k_r a) + J_{n-2}(k_r a)] - [J_{n+2}(k_l a) - J_{n-2}(k_l a)] \times [J_{n+2}(k_r a) - J_{n-2}(k_r a)] = 0. \quad (107)$$

Thus the normalized surface-wave frequency $\omega_S a/v_t$ divided

FIG. 6. (Color online) Lattice displacements of the edge mode (the even solution with $\omega a/v_t = 19.38$). (a) u_r , (b) u_θ , and (c) u_z on the top surface $z=h$ of the disk. (d) Displacement amplitudes (u_r, u_θ, u_z) versus distance r (along the line at $\theta=25^\circ$) from the center on the top surface $z=h$. Inset shows $J_{n=20}(x)$ (solid line) versus x/n and its asymptotic formulas (dotted lines) by Debye. For x_0 and x_1 , see the text. Angular wave number is $n=20$ and aspect ratio is $h/a=0.5$.

by the angular wave number n that is equivalent to the ratio of surface-wave velocity $v_S = \omega_S a/n$ on the curved surface to v_t , or $\omega_S a/v_t n = v_S/v_t$, is obtained by solving Eq. (107). The result is displayed also in Fig. 5 by crosses. We see that the surface-wave velocity v_S decreases with increasing n similar to the cases of the edge modes. In the limit of large n , the following formula holds for the Bessel functions with argument less than the order n (with $\alpha > 0$):³⁰

$$J_n(n \operatorname{sech} \alpha) \sim \frac{1}{(2\pi n \tanh \alpha)^{1/2}} e^{n(\tanh \alpha - \alpha)}, \quad (108)$$

or equivalently

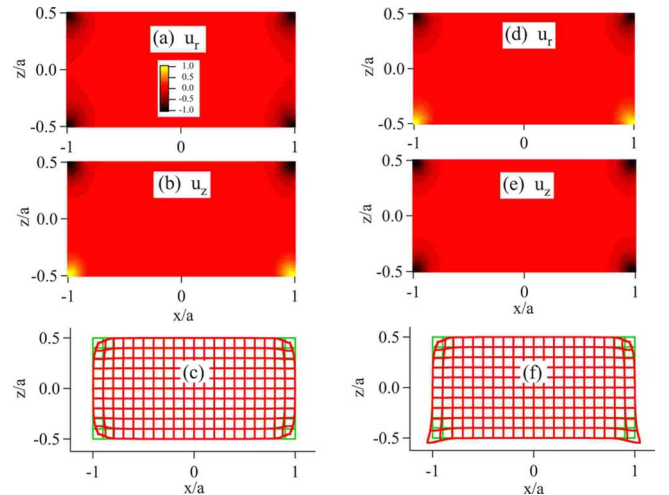


FIG. 7. (Color online) Displacement profiles of the edge modes. (a) u_r and (b) u_z in the x - z plane (the section at $\theta=0^\circ$) of the even solution ($\omega a/v_t=19.38$). (c) Comparison of the displaced (red bold line) and undisplaced (green thin line) lattices of the even solution in the same plane of the disk. The corresponding results for the odd solution ($\omega a/v_t=19.36$) are shown in (d)–(f). Angular wave number is $n=20$ and aspect ratio is $h/a=0.5$.

$$J_n(x) \sim \frac{1}{\sqrt{2\pi(n^2-x^2)^{1/4}}} e^{\sqrt{n^2-x^2}-n \cosh^{-1}(n/x)}, \quad (109)$$

where $n > x \gg 1$. With this formula, Eq. (107) is reduced to

$$(2k^2 - k_t^2)^2 - 4k^2(k^2 - k_t^2)^{1/2}(k^2 - k_t^2)^{1/2} = 0. \quad (110)$$

This is the well-known equation for determining the velocity $v_R = \omega/k$ ($k = n/a$) of the Rayleigh surface waves on the free, flat surface of an isotropic elastic medium.³⁵ It should be noted that the equation $n = ka$ and finite k mean that $n \rightarrow \infty$ and $a \rightarrow \infty$ are equivalent to each other. From Eq. (110) we find $v_R/v_t = 0.934$ for aluminum as indicated in Fig. 5. This figure also shows that the velocity of the edge modes, v_E ($v_E/v_t = 0.907$), in the limit of large n is slower than v_R . This is consistent with the result given by Maradudin *et al.*³³ on the speed of the edge-mode waves.

Figure 5 also suggests that $v_l > v_s > v_t$ for $n \leq 22$. This means that the velocity v_s is faster than v_t and the modes in the second lowest branches (both the even and odd solutions) are not true surface modes which consist only of the wave components localized near the circumferential surface. The transverse components of these modes for $n \leq 22$ are extended but they are still trapped near the surface by repeating the total internal reflections from the curved surface, i.e., these vibrational modes correspond to the whispering-gallery (WG) modes.¹⁸ For $n \geq 23$, however, $v_t > v_s$ holds and the modes are truly Rayleigh type consisting of only localized wave components.

D. Profiles of the lattice displacements for the angular wave number $n=20$: Edge modes and surface modes

More detailed information on the vibrations of the low-lying branches at a large n is obtained from the profiles of the associated lattice displacements \mathbf{u} . For illustration, we consider two typical disks with aspect ratios $h/a = 0.5$ and 0.05 . For the former value of h/a , the lowest frequencies of both the even and odd solutions are nearly identical and equal to the edge-mode frequency ω_E (Fig. 3). However, for the latter value $h/a = 0.05$, the lowest frequencies of those two solutions are quite different and change rather sensitively as h/a varies.

1. $h/a = 0.5$

Figure 6 shows, for the disk with $h/a = 0.5$, the profiles of the displacement amplitudes \mathbf{u} in the x - y plane (on the top surface at $z = h$) of the lowest mode at $\omega a/v_t = 19.38$ ($n = 20$). The results displayed are for the even solution calculated with $N_r = N_z = 5$ but no difference (other than the sign of the amplitudes) is discernible for the odd solution because their eigenfrequencies are essentially coincident for $h/a = 0.5$ assumed. As n increases the vibrational motions of the lattices are centrifugally pushed toward the cylindrical surface and the lattice displacement \mathbf{u} for $n = 20$ is well localized near the circumference $r = a$. We also see that u_r and u_z components dominate the component u_θ . More quantitatively, the displacement components in the vertical plane $\theta = 25^\circ$ rotated away from the x - z plane are compared in Fig. 6(d). (Note that u_θ is identically zero at $\theta = 0^\circ$.)

Here we estimate the distance from the cylindrical surface over which the displacement amplitudes are trapped in the radial direction. For this purpose we again use asymptotic formula (108) and also another one for the Bessel functions with large n ,³⁰

$$J_n(n \sec \beta) \sim \frac{2}{(\pi n \tan \beta)^{1/2}} \cos \left[n(\tan \beta - \beta) - \frac{\pi}{4} \right], \quad (111)$$

which is valid for the argument larger than the order n . This equation is equivalent to

$$J_n(x) \sim \frac{2}{\sqrt{2\pi(x^2 - n^2)^{1/4}}} \cos \left[\sqrt{x^2 - n^2} - n \cos^{-1} \left(\frac{n}{x} \right) - \frac{\pi}{4} \right], \quad (112)$$

where $1 \ll n < x$. Equations (109) and (112) are illustrated in the inset of Fig. 6(d) labeled as ‘‘Debye’s formulas.’’³⁴

Now, for a large n , the minimum root $x = x_1$ of $J'_n(x) = 0$ that gives the local maximum of $J_n(x)$ is $x_1 = n + 0.8086n^{1/3} + o(n^{-1/3})$ [Eq. (103)] and Eq. (112) gives (by setting $\gamma = 0.8086$)

$$\begin{aligned} J_n(x_1) &= J_n(n + \gamma n^{1/3}) \sim \left(\frac{2}{\pi^2 \gamma} \right)^{-1/4} n^{-1/3} \cos \left(\frac{2\sqrt{2}}{3} \gamma^{3/2} - \frac{\pi}{4} \right) \\ &= 0.704n^{-1/3}. \end{aligned} \quad (113)$$

Next, we tentatively calculate $J_n(x)$ at $x = x_0 \equiv n - \gamma n^{1/3}$. With Eq. (109) we find

$$\begin{aligned} J_n(x_0) &= J_n(n - \gamma n^{1/3}) \sim \left(\frac{1}{8\pi^2 \gamma} \right)^{-1/4} n^{-1/3} \exp \left(\frac{2\sqrt{2}}{3} \gamma^{3/2} \right) \\ &= 0.178n^{-1/3}. \end{aligned} \quad (114)$$

Thus, $J_n(x_0) \approx J_n(x_1)/4$ and $J_n(x)$ decreases exponentially as x decreases in the region $x < x_0$. From these considerations we can deduce that the displacement amplitudes are confined in the region $r/a = 1 - 2\gamma n^{-2/3}$ ($= 1 - |x_1 - x_0|/n$) $= 1 - 1.61n^{-2/3} \sim 1$ in the radial direction. This means that the vibrations are trapped in the ranges $r/a = 0.78 \sim 1$ for $n = 20$ and $r/a = 0.93 \sim 1$ for $n = 100$. Figure 6(d) shows that all three components of the lattice displacement \mathbf{u} are really localized within this region for $n = 20$.

Figure 7 displays the similar profiles of u_r and u_z (both the even and odd solutions) in the x - z plane with $\theta = 0$ ($u_\theta = 0$). This figure shows that the displacement \mathbf{u} is also confined in the vicinity of $z = \pm h$ ($= \pm a/2$), indicating that the vibrations of the lowest two branches are the modes localized at the circular edges of the cylindrical disk. The situation does not change for a thicker disk with $h/a > 0.5$ as suggested by the flatness of the branches shown in Fig. 3. For the modes well trapped near the edges of a thick disk, the symmetry and antisymmetry of the displacement amplitudes with respect to $z = 0$ are irrelevant and hence do not yield any difference in the eigenfrequencies of the even and odd solutions.

In the second lowest set of the branches, the lattice displacements are considerably different from those of the lowest edge modes. The profiles of u_r and u_z in the x - z plane with $\theta = 0$ are illustrated in Fig. 8 also for the disk with

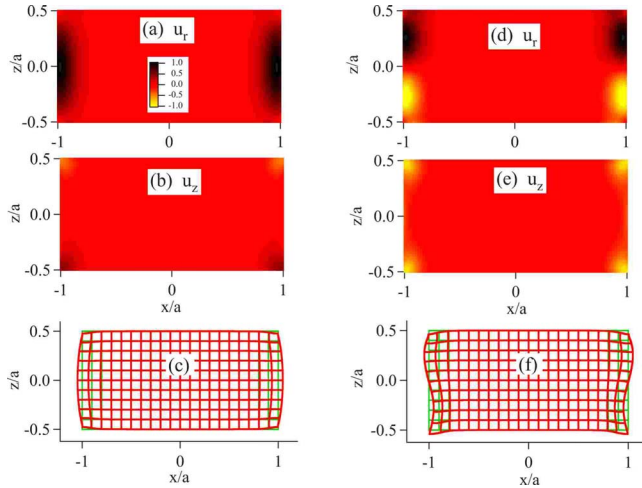


FIG. 8. (Color online) Displacement profiles of the surface modes. (a) u_r and (b) u_z in the x - z plane (the section at $\theta=0^\circ$) of the even solution ($\omega a/v_t=20.37$). (c) Comparison of the displaced (red bold line) and undisplaced (green thin line) lattices of the even solution in the same plane of the disk. The corresponding results for the odd solution ($\omega a/v_t=20.80$) are shown in (d)–(f). Angular wave number is $n=20$ and aspect ratio is $h/a=0.5$.

$h/a=0.5$. We see that they are still localized near the cylindrical surface $r=a$ but not necessarily near the edges $z=\pm h$. The larger component u_r is rather extended over $-h \leq z \leq h$ on the cylindrical surface $r=a$. The even and odd solutions do not have the same frequency anymore for the same aspect ratio $h/a (=0.5)$ because the presence or absence of a node at $z=0$ in the displacement plays an important role in determining the eigenfrequencies. Explicitly, their values at $h/a=0.5$ are $\omega a/v_t=20.37$ for the even solution and $\omega a/v_t=20.80$ for the odd solution.

2. $h/a=0.05$

For comparison, we have also calculated u_r and u_z in the x - z plane for the thinner disk with aspect ratio $h/a=0.05$. This value is close to the lower limit for typical microdisks fabricated for photonic cavities ($h/a=0.1-0.05$).¹⁰ Contrary to the case of $h/a=0.5$, the lowest resonant frequencies of both the even and odd solutions for this thin disk are found in the region where they change sensitively depending on h/a , or the disk thickness (Figs. 3 and 4). This fact suggests that the corresponding mode amplitudes are not confined at the edges near the top and bottom faces of the disk but rather extended over the thickness direction.

Figure 9 shows that this is really the case and we recognize that the even solution [Figs. 9(a) and 9(b)] for this thin circular disk (with the larger eigenfrequency $\omega a/v_t=19.88$) is a dilatational mode vibrating mainly in the radial direction ($|u_r| > |u_z|$) but only near the circumference $r=a$ of the disk (i.e., a mode still localized near the cylindrical surface because of a large angular wave number n). At the same time, this vibration is associated with small contraction and expansion along the thickness direction z that are also confined near the edges. In contrast, the odd solution [Fig. 9(c)] with a smaller resonant frequency ($\omega a/v_t=14.66$) is a bending

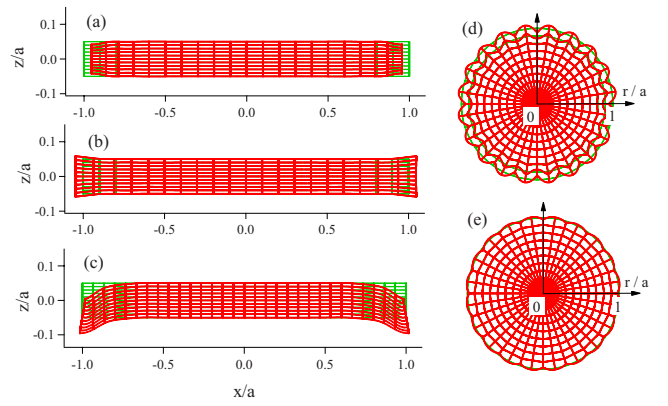


FIG. 9. (Color online) Comparison of the displaced (red bold line) and undisplaced (green thin line) lattices in a thin disk with aspect ratio $h/a=0.05$. The lowest frequency modes with angular wave number $n=20$ are illustrated. (a) The even solution at $\omega a/v_t=19.88$ in the x - z plane (the section at $\theta=0^\circ$ of the disk). (b) The same as (a) but in the plane at $\theta=90^\circ$ of the disk. (c) The odd solution at $\omega a/v_t=14.66$ in the x - z plane (the section at $\theta=0^\circ$ of the disk). (d) The even solution at $\omega a/v_t=19.88$ on the top face $z=h$ of the disk. (e) The odd solution at $\omega a/v_t=14.66$ on the top face $z=h$ of the disk.

(flexural) mode vibrating predominantly in the thickness direction ($|u_z| > |u_r|$) localized near $r=a$. No local volume change is accompanied by this mode. We have also shown in Figs. 9(d) and 9(e) the profiles of the lattice displacements at the top face $z=h$ of the disk, for the even and odd solutions, respectively.

Finally, we note that at the frequencies in higher branches the vibrations in both the even and odd solutions have nodes in the radial direction. The existence of these nodes means that the vibrational amplitudes are extended from the cylindrical surface toward the center $r=0$ of the circular plane and the associated strain energies are also extended in the disk.

VI. SUMMARY AND DISCUSSIONS

We have studied the vibrational properties of low-lying resonant modes confined in a small volume near the edges and the circumference of a free cylindrical disk. This has been done by constructing the lattice displacements by summing the relevant solutions of equations of motion, so that they may satisfy the stress-free boundary conditions at the boundary surfaces of the disk. The formulation employed was originally considered by Rasband²¹ and Hutchinson²⁵ and apparently looks complicated. However, the numerical calculation is rather straightforward and the eigenfrequencies are obtained by finding zeros of the determinant of a matrix with unexpectedly small rank. An advantage of this method is the fact that the vibrational modes are calculated for a given angular wave number n , which is not straightforward with the RUS and finite element methods.

With the present formulation we have concentrated on the vibrations with a large angular wave number n and found the existence of doubly degenerate edge modes (consisting of the even and odd solutions of the same frequencies) for a

thick disk with aspect ratios $h/a > 0.5$. Their eigenfrequencies are well separated from those of the upper branches including the surface modes. For $h/a < 0.5$, however, this degeneracy is lifted and the frequency of the even (odd) solution increases (decreases) and the vibration is dilatational (flexural) localized near the side wall of the disk.

Our goal is to develop a systematic formulation to analyze the vibrational properties of micro- and nanoelastic cavities. The formulation we have employed for a freestanding disk can basically be extended and applied to more complicated elastic small structures with free surfaces, such as a thin disk consisting of double layers and more generally of multilayers composed of dissimilar solids stacked in the axial direction. In particular, we plan to study theoretically the vibrational properties of a perfect periodic circular pillar and also more interesting micro- and nanopillars (with or without a cavity layer) that can be used for pumping SASERs of small dimensions.

Finally, we note that the present formulation for satisfying the matching conditions at boundary surfaces oriented in different directions can be also applied to analyze the scattering of sound waves from an elastic body.³⁶ Specifically, an interesting subject is the scattering in phononic crystals³⁷ consisting of particles of a cylindrical shape embedded periodically in a dissimilar elastic background.

ACKNOWLEDGMENTS

This work was supported in part by the Grant-in-Aid for Scientific Research from the Ministry of Education, Science, Sports and Culture of Japan (Grant No. 17510106).

APPENDIX A: EXPRESSIONS FOR S_n^r AND S_n^z

The expressions for the elements of the matrix S_n^r describing the stresses T_{rr} , $T_{r\theta}$, and T_{rz} are

$$(S_n^r)_{11} = \left[q^2 - \frac{\omega^2}{2v_t^2} + \frac{\chi_n(k,r)}{r^2} \right] J_n(k,r) \begin{pmatrix} \cos qz \\ \sin qz \end{pmatrix} \cos n\theta, \quad (\text{A1})$$

$$(S_n^r)_{12} = -\frac{n}{r^2} f_n(k,r) J_n(k,r) \begin{pmatrix} \cos qz \\ \sin qz \end{pmatrix} \cos n\theta, \quad (\text{A2})$$

$$(S_n^r)_{13} = \frac{q}{r^2} [(k,r)^2 - \chi_n(k,r)] J_n(k,r) \begin{pmatrix} \cos qz \\ \sin qz \end{pmatrix} \cos n\theta, \quad (\text{A3})$$

$$(S_n^r)_{21} = -\frac{n}{r^2} f_n(k,r) J_n(k,r) \begin{pmatrix} \cos qz \\ \sin qz \end{pmatrix} \sin n\theta, \quad (\text{A4})$$

$$(S_n^r)_{22} = \frac{1}{r^2} \left[-\frac{1}{2}(k,r)^2 + \chi_n(k,r) \right] J_n(k,r) \begin{pmatrix} \cos qz \\ \sin qz \end{pmatrix} \sin n\theta, \quad (\text{A5})$$

$$(S_n^r)_{23} = \frac{nq}{r^2} f_n(k,r) J_n(k,r) \begin{pmatrix} \cos qz \\ \sin qz \end{pmatrix} \sin n\theta, \quad (\text{A6})$$

$$(S_n^r)_{31} = qk_r J_n'(k,r) \begin{pmatrix} -\sin qz \\ \cos qz \end{pmatrix} \cos n\theta, \quad (\text{A7})$$

$$(S_n^r)_{32} = -\frac{nq}{2r} J_n(k,r) \begin{pmatrix} -\sin qz \\ \cos qz \end{pmatrix} \cos n\theta, \quad (\text{A8})$$

$$(S_n^r)_{33} = \frac{k_t}{2} (k_t^2 - q^2) J_n'(k,r) \begin{pmatrix} -\sin qz \\ \cos qz \end{pmatrix} \cos n\theta. \quad (\text{A9})$$

In these equations we have introduced $f_n(x)$ and $\chi_n(x)$ defined by

$$f_n(x) \equiv xJ_{n-1}(x)/J_n(x) - (n+1), \quad (\text{A10})$$

$$\chi_n(x) \equiv n^2 + n - xJ_{n-1}(x)/J_n(x). \quad (\text{A11})$$

We note that for an imaginary argument $f_n(ix) = xI_{n-1}(x)/I_n(x) - (n+1)$ and so on. The expressions for the elements of the matrix S_n^z describing the stresses T_{zr} , $T_{z\theta}$, and T_{zz} are

$$(S_n^z)_{11} = qk_r J_n'(k,r) \begin{pmatrix} -\sin qz \\ \cos qz \end{pmatrix} \cos n\theta, \quad (\text{A12})$$

$$(S_n^z)_{12} = -\frac{nq}{2r} J_n(k,r) \begin{pmatrix} -\sin qz \\ \cos qz \end{pmatrix} \cos n\theta, \quad (\text{A13})$$

$$(S_n^z)_{13} = \frac{1}{2} k_t (k_t^2 - q^2) J_n'(k,r) \begin{pmatrix} -\sin qz \\ \cos qz \end{pmatrix} \cos n\theta, \quad (\text{A14})$$

$$(S_n^z)_{21} = -\frac{nq}{r} J_n(k,r) \begin{pmatrix} -\sin qz \\ \cos qz \end{pmatrix} \sin n\theta, \quad (\text{A15})$$

$$(S_n^z)_{22} = \frac{qk_t}{2} J_n'(k,r) \begin{pmatrix} -\sin qz \\ \cos qz \end{pmatrix} \sin n\theta, \quad (\text{A16})$$

$$(S_n^z)_{23} = \frac{n}{2r} (q^2 - k_t^2) J_n(k,r) \begin{pmatrix} -\sin qz \\ \cos qz \end{pmatrix} \sin n\theta, \quad (\text{A17})$$

$$(S_n^z)_{31} = \left(k_t^2 - \frac{\omega^2}{2v_t^2} \right) J_n(k,r) \begin{pmatrix} \cos qz \\ \sin qz \end{pmatrix} \cos n\theta, \quad (\text{A18})$$

$$(S_n^z)_{32} = 0, \quad (\text{A19})$$

$$(S_n^z)_{33} = -qk_t^2 J_n(k,r) \begin{pmatrix} \cos qz \\ \sin qz \end{pmatrix} \cos n\theta. \quad (\text{A20})$$

APPENDIX B: EXPRESSIONS FOR \tilde{S}_n^r AND \tilde{S}_n^z

The expressions for the elements of \tilde{S}_n^r and \tilde{S}_n^z are

$$(\tilde{S}_n^r)_{11} = \left[q_l^2 - \frac{\omega^2}{2v_l^2} + \frac{\chi_n(k,r)}{r^2} \right] J_n(k,r) \begin{pmatrix} \cos q_l z \\ \sin q_l z \end{pmatrix} \cos n\theta, \quad (\text{B1})$$

$$(\tilde{S}_n^r)_{12} = -\frac{n}{r^2} f_n(kr) J_n(kr) \begin{pmatrix} \cos q_r z \\ \sin q_r z \end{pmatrix} \cos n\theta, \quad (\text{B2})$$

$$(\tilde{S}_n^r)_{13} = \frac{q_t}{r^2} [(kr)^2 - \chi_n(kr)] J_n(kr) \begin{pmatrix} \cos q_t z \\ \sin q_t z \end{pmatrix} \cos n\theta, \quad (\text{B3})$$

$$(\tilde{S}_n^r)_{21} = -\frac{n}{r^2} f_n(kr) J_n(kr) \begin{pmatrix} \cos q_r z \\ \sin q_r z \end{pmatrix} \sin n\theta, \quad (\text{B4})$$

$$(\tilde{S}_n^r)_{22} = \frac{1}{r^2} \left[-\frac{(kr)^2}{2} + \chi_n(kr) \right] J_n(kr) \begin{pmatrix} \cos q_r z \\ \sin q_r z \end{pmatrix} \sin n\theta, \quad (\text{B5})$$

$$(\tilde{S}_n^r)_{23} = \frac{nq_t}{r^2} f_n(kr) J_n(kr) \begin{pmatrix} \cos q_t z \\ \sin q_t z \end{pmatrix} \sin n\theta, \quad (\text{B6})$$

$$(\tilde{S}_n^r)_{31} = q_l k J_n'(kr) \begin{pmatrix} -\sin q_l z \\ \cos q_l z \end{pmatrix} \cos n\theta, \quad (\text{B7})$$

$$(\tilde{S}_n^r)_{32} = -\frac{nq_t}{2r} J_n(kr) \begin{pmatrix} -\sin q_t z \\ \cos q_t z \end{pmatrix} \cos n\theta, \quad (\text{B8})$$

$$(\tilde{S}_n^r)_{33} = \frac{k}{2} (k^2 - q_t^2) J_n'(kr) \begin{pmatrix} -\sin q_t z \\ \cos q_t z \end{pmatrix} \cos n\theta, \quad (\text{B9})$$

$$(\tilde{S}_n^z)_{11} = q_l k J_n'(kr) \begin{pmatrix} -\sin q_l z \\ \cos q_l z \end{pmatrix} \cos n\theta, \quad (\text{B10})$$

$$(\tilde{S}_n^z)_{12} = -\frac{nq_t}{2r} J_n(kr) \begin{pmatrix} -\sin q_t z \\ \cos q_t z \end{pmatrix} \cos n\theta, \quad (\text{B11})$$

$$(\tilde{S}_n^z)_{13} = \frac{1}{2} k (k^2 - q_t^2) J_n'(kr) \begin{pmatrix} -\sin q_t z \\ \cos q_t z \end{pmatrix} \cos n\theta, \quad (\text{B12})$$

$$(\tilde{S}_n^z)_{21} = -\frac{nq_l}{r} J_n(kr) \begin{pmatrix} -\sin q_l z \\ \cos q_l z \end{pmatrix} \sin n\theta, \quad (\text{B13})$$

$$(\tilde{S}_n^z)_{22} = \frac{q_t k}{2} J_n'(kr) \begin{pmatrix} -\sin q_t z \\ \cos q_t z \end{pmatrix} \sin n\theta, \quad (\text{B14})$$

$$(\tilde{S}_n^z)_{23} = -\frac{n}{2r} (k^2 - q_t^2) J_n(kr) \begin{pmatrix} -\sin q_t z \\ \cos q_t z \end{pmatrix} \sin n\theta, \quad (\text{B15})$$

$$(\tilde{S}_n^z)_{31} = \frac{1}{2} (k^2 - q_t^2) J_n(kr) \begin{pmatrix} \cos q_l z \\ \sin q_l z \end{pmatrix} \cos n\theta, \quad (\text{B16})$$

$$(\tilde{S}_n^z)_{32} = 0, \quad (\text{B17})$$

$$(\tilde{S}_n^z)_{33} = -q_t k^2 J_n(kr) \begin{pmatrix} \cos q_t z \\ \sin q_t z \end{pmatrix} \cos n\theta. \quad (\text{B18})$$

- ¹H.-N. Lin, H. J. Maris, L. B. Freund, K. Y. Lee, H. Luhn, and D. P. Kern, *J. Appl. Phys.* **73**, 37 (1993).
²G. A. Antonelli, H. J. Maris, S. G. Malhotra, and J. M. E. Harper, *J. Appl. Phys.* **91**, 3261 (2002).
³T. Bienville, J. F. Robillard, L. Belliard, I. Roch-Jeune, A. Devos, and B. Perrin, *Ultrasonics* **44**, e1289 (2006).
⁴C. Giannetti, B. Revaz, F. Banfi, M. Montagnese, G. Ferrini, F. Cilento, S. Moccagli, P. Vavassori, G. Oliviero, E. Bontempi, L. E. Depero, V. Metlushko, and F. Parmigiani, *Phys. Rev. B* **76**, 125413 (2007).
⁵A. V. Akimov, Y. Tanaka, A. B. Pevtsov, S. F. Kaplan, V. G. Golubev, S. Tamura, D. R. Yakovlev, and M. Bayer, *Phys. Rev. Lett.* **101**, 033902 (2008).
⁶W. Cheng, J. J. Wang, U. Jonas, G. Fytas, and N. Stefanou, *Nature Mater.* **5**, 830 (2006).
⁷T. Still, W. Cheng, M. Retsch, R. Sainidou, J. Wang, U. Jonas, N. Stefanou, and G. Fytas, *Phys. Rev. Lett.* **100**, 194301 (2008).
⁸M. Blencowe, *Phys. Rep.* **395**, 159 (2004).
⁹R. N. Kini, N. M. Stanton, A. Kent, and M. Henini, *Phys. Status Solidi C* **1**, 2682 (2004).
¹⁰J. M. Gerard, *Nature Mater.* **2**, 140 (2003).
¹¹J. M. Gerard, B. Sermage, B. Gayral, B. Legrand, E. Costard, and V. Thierry-Mieg, *Phys. Rev. Lett.* **81**, 1110 (1998).
¹²A. Kiraz, P. Michler, C. Becher, B. Gayral, A. Imamoglu, Li-dong Zhang, and E. Hu, *Appl. Phys. Lett.* **78**, 3932 (2001).

- ¹³D. K. Armani, T. J. Kippenberg, S. M. Spillane, and K. J. Vahala, *Nature Mater.* **421**, 925 (2003).
¹⁴V. N. Astratov, S. Yang, S. Lam, B. D. Jones, D. Sanvitto, D. M. Whittaker, A. M. Fox, M. S. Skolnick, A. Tahraoui, P. W. Fry, and M. Hopkinson, *Appl. Phys. Lett.* **91**, 071115 (2007).
¹⁵I. A. Viktorov, *Akust. Zh.* **4**, 131 (1958); [*Sov. Phys. Acoust.* **4**, 131 (1958)].
¹⁶B. Rulf, *J. Acoust. Soc. Am.* **45**, 493 (1969).
¹⁷Lord Rayleigh, *Theory of Sound*, 2nd ed. (Dover, New York, 1945).
¹⁸L. M. Brekhovskikh, *Akust. Zh.* **13**, 541 (1967) [*Sov. Phys. Acoust.* **13**, 462 (1968)].
¹⁹With this localized nature of the vibrational modes studied, the presence of the column that supports the central part of a circular microdisk fabricated should be irrelevant in the present analysis for large n .
²⁰Unlike the case of the electromagnetic waves, the leakage of the vibrational field outside the disk does not exist for the present structure.
²¹S. N. Rasband, *J. Acoust. Soc. Am.* **57**, 899 (1975).
²²W. M. Visscher, A. Magliori, T. M. Bell, and R. A. Reinert, *J. Acoust. Soc. Am.* **90**, 2154 (1991).
²³M. Petyt, *Introduction to Finite Element Vibration Analysis* (Cambridge University Press, New York, 1990).
²⁴J. R. Hutchinson, *J. Acoust. Soc. Am.* **51**, 233 (1972).

- ²⁵J. R. Hutchinson, *J. Appl. Mech.* **47**, 901 (1980).
- ²⁶Our method combines two series of exact solutions for the lattice displacements but Hutchinson (Ref. 25) used three series of the solutions.
- ²⁷Another set of solutions is possible by interchanging $\cos n\theta$ and $\sin n\theta$. They will be used for the torsional mode with $n=0$.
- ²⁸These relations are derived with the recurrence relation of the Bessel function $(d/dx+n/x)J_n(x)=J_{n-1}(x)$.
- ²⁹For Bessel functions the following equations hold with α and β as arbitrary constants: $(\alpha^2-\beta^2)\int_0^a r J_n(\alpha r) J_n(\beta r) dr = a[\beta J_n(\alpha a) J_n'(\beta a) - \alpha J_n(\beta a) J_n'(\alpha a)]$ and $\int_0^a r [J_n(\beta r)]^2 dr = (a^2/2)\{[J_n'(\beta a)]^2 + [1-n^2/(\beta a)^2][J_n(\beta a)]^2\}$.
- ³⁰G. N. Watson, *Theory of Bessel Functions*, 2nd ed. (Cambridge University Press, New York, 1966).
- ³¹K. F. Graff, *Wave Motion in Elastic Solids* (Dover, New York, 1975).
- ³²G. W. McMahon, *J. Acoust. Soc. Am.* **36**, 85 (1964).
- ³³A. A. Maradudin, R. F. Wallis, D. L. Mills, and R. L. Ballard, *Phys. Rev. B* **6**, 1106 (1972).
- ³⁴*Handbook of Mathematical Functions*, edited by M. Abramovitz and I. A. Stegun (Dover, New York, 1964).
- ³⁵G. W. Farnell, in *Physical Acoustics VI*, edited by W. P. Mason and R. N. Thurston (Academic, New York, 1970), p. 109.
- ³⁶P. C. Waterman, *J. Acoust. Soc. Am.* **60**, 567 (1976).
- ³⁷R. Sainidou, N. Stefanou, I. E. Psarobas, and A. Modinos, *Comput. Phys. Commun.* **166**, 197 (2005).